

1 Satellite Detection of NO₂ Distributions Using TROPOMI and 2 TEMPO and Comparison with Ground-Based Concentrations

4 Summer Acker,¹ Tracey Holloway^{1, 2} and Monica Harkey¹

5 ¹ Nelson Institute Center for Sustainability and the Global Environment, University of Wisconsin-Madison,
6 Madison, WI 53705, United States of America

7 ² Department of Atmospheric and Oceanic Sciences, University of Wisconsin-Madison, Madison, WI 53705, United
8 States of America

10 *Correspondence to:* Tracey Holloway (taholloway@wisc.edu)

12 Abstract

13 In this study we assess the capability of current-generation satellites to capture the variability of
14 near-surface nitrogen dioxide (NO₂) monitoring data, with the goal of supporting health and
15 regulatory applications. We consider NO₂ vertical column densities (VCD) over the United
16 States from two satellite instruments, the Tropospheric Monitoring Instrument (TROPOMI), and
17 Tropospheric Emissions: Monitoring of Pollution (TEMPO), and compare with ground-based
18 concentrations as measured by the EPA's Air Quality System (AQS) monitors. While
19 TROPOMI provides a longer-term record of assessment (2019-2023), TEMPO informs diurnal
20 patterns relevant to evaluating peak NO₂. We analyze frequency distributions and quantify their
21 similarity using the Jensen-Shannon Divergence (JSD), where smaller values indicate better
22 agreement. Satellite and ground monitor NO₂ distributions are most similar at non-roadway
23 monitors away from major roads (JSD = 0.008), as indicated by the JSD of 0.008 calculated for
24 TROPOMI and ground monitors at non-roadways, compared with a JSD near and are most
25 different at interstates of (JSD = 0.158) and a JSD near highways of (JSD = 0.095) monitors.
26 Seasonal analysis shows the most similarity in distributions in winter (JSD = , with a JSD of
27 0.010), and the most difference in summer, with a (JSD = 0.035). Across seasons and monitor
28 locations, the calculated 1:30pm LT TEMPO consistently exhibits has a lower or similar
29 comparable JSDs to as TROPOMI, with (TEMPO: JSDs ranging from 0.005 to 0.151; and

30 TROPOMI: ~~JSDs ranging from~~ 0.012 to 0.265). TEMPO's agreement with monitors in both
31 December 2023 and July 2024 is found to be best around midday, with non-road monitors' ~~JSD~~
32 in July ~~having theas best alignmentlow as (JSD = 0.008)~~ at 16 UTC (~11am LT). ~~These findings~~
33 ~~highlight the ability of TROPOMI and TEMPO to complement existing ground-based monitors,~~
34 ~~and demonstrate their potential for monitor siting, regulatory, and public health applications.~~

35 1 Introduction

36 ~~The frequency distribution of ambient pollutants in urban areas has long been recognized as a~~
37 ~~useful metric for comparison with health-based thresholds, and to assess the effectiveness of~~
38 ~~emission controls. Early studies found pollutant concentrations in urban areas to be~~
39 ~~approximately lognormally distributed (Knox and Lange, 1974; Pollack, 1975; Venkatram,~~
40 ~~1979) and isolated point sources better described by exponential distributions (Venkatram,~~
41 ~~1979). The distributional lens also bears relevance to advanced health and regulatory assessment~~
42 ~~(Chowdhury et al., 2021; Mondal et al., 2021). In this study we evaluate the capability of current~~
43 ~~generation satellites to capture the variability of near-surface nitrogen dioxide (NO₂) monitoring~~
44 ~~data, with the goal of supporting health and regulatory applications.~~

45 Nitrogen dioxide (NO₂) is a gas released through high temperature combustion processes such as
46 the burning of fossil fuels (Lee et al., 1997; Richter et al., 2005), with on-road vehicles, power
47 plants, and industrial processes representing the largest anthropogenic sources in the United
48 States (U.S.; van der A et al., 2008) as well as lightning NO_x emissions (Dang et al., 2023) and
49 soil microbial activity (Huber et al., 2020) from natural sources. Exposure to elevated levels of
50 NO₂ has been linked to respiratory and cardiovascular diseases (Mills et al., 2015; Urbanowicz et
51 al., 2023; Meng et al., 2021), especially asthma in children (Mölter et al., 2014; Anenberg et al.,
52 2022; Achakulwisut et al., 2019), as well as premature mortality (Camilleri et al., 2023; Hales et
53 al., 2021; Huangfu and Atkinson, 2020), and other diseases (Xia et al., 2024; Bai et al., 2018).
54 NO₂ plays a critical role in the formation of ozone, which also causes respiratory health problems
55 and is harmful to ecosystems (Grulke & Heath, 2019; Sillman, 1999). It is also a precursor to
56 nitrate (Behera & Sharma, 2012), a type of fine particulate matter (PM_{2.5}), which can penetrate
57 deep into the lungs and exacerbate respiratory and heart conditions (Sangkham et al., 2024;

58 Sharma et al., 2020), as well as cause premature death (Orellano et al., 2020; Thangavel et al.,
59 2022).

60 ~~The EPA Air Quality System (AQS) contains hourly NO₂ measurements from ground-based~~
61 ~~monitors, providing high temporal resolution data that are critical for assessing compliance with~~
62 ~~the U.S. National Ambient Air Quality Standards (NAAQS). There are two NAAQS related to~~
63 ~~NO₂: one for annual average concentration, set at 53 ppb, and one based on peak 1-hour~~
64 ~~concentrations, set at 100 ppb, based on the 3-year average of the 98th percentile of the yearly~~
65 ~~distribution of 1-hour daily maximum NO₂ concentrations (EPA, 2010). Enforcement of these~~
66 ~~standards relies on data from AQS NO₂ monitors, a network that includes 431 monitors as of~~
67 ~~2024. Because NO₂ has a relatively short atmospheric lifetime, typically ranging from a few~~
68 ~~hours to a day depending on meteorological conditions (Lange et al., 2022; Liu et al., 2021),~~
69 ~~ground monitors are expected to capture local conditions (Wang et al., 2020).~~

70 ~~Several studies have highlighted the potential for satellite NO₂ data to supplement ground-based~~
71 ~~networks (Duncan et al., 2014; Lee & Koutrakis, 2014). Due to its radiative characteristics, NO₂~~
72 ~~may be observed by satellites during daylight hours (Boersma et al., 2018; Van Geffen et al.,~~
73 ~~2020; Veefkind et al., 2012), and NO₂ has emerged as one of the most air-quality-relevant~~
74 ~~pollutants from satellites (Holloway et al., 2021). Several studies have highlighted the potential~~
75 ~~for satellite NO₂ data to supplement ground-based networks to support health analysis and air~~
76 ~~quality management (Duncan et al., 2014; Lee & Koutrakis, 2014). Some of the first studies~~
77 ~~done comparing ground-based NO₂ to satellite VCDs (Lamsal et al., 2014; Lamsal et al., 2015;~~
78 ~~Zhang et al., 2018) used the Ozone Monitoring Instrument (OMI, 13 km × 24 km; Levelt et al.,~~
79 ~~2006). Annual OMI and surface NO₂ trends in the U.S. show that OMI usually overestimates the~~
80 ~~surface trends by ~3.7% each year (Zhang et al., 2018). With the 2017 launch of the~~
81 ~~Tropospheric Monitoring Instrument (TROPOMI; Boersma et al., 2018; Van Geffen et al., 2020;~~
82 ~~Veefkind et al., 2012), new opportunities arose for analyzing column to surface agreement at a~~
83 ~~higher resolution (3.5 km × 5.5 km) advanced these applications (Goldberg et al., 2021; Griffin et~~
84 ~~al., 2019; Kim et al., 2024; Yu & Li, 2022; Dressel et al., 2022; Goldberg et al., 2024; H. J. Lee~~
85 ~~et al., 2023). The Tropospheric Emissions: Monitoring of Pollution (TEMPO; Chance et al.,~~
86 ~~2019; Naeger et al., 2021; Zoogman et al., 2017) provides further advancements with daytime~~
87 ~~hourly observations of NO₂ over North America and finer spatial coverage.~~

88 While advanced methods exist to calculate near-surface NO₂ explicitly (Ahmad et al., 2024; Kim
89 et al., 2021; Shetty et al., 2024; Virta et al., 2023), there is also a strong interest in the utilization
90 of satellite vertical column density (VCD) to directly infer NO₂ concentrations analogous to
91 ground-based monitors (Kim et al., 2024; Lamsal et al., 2014; Griffin et al., 2019; Yu & Li,
92 2022; Zhang et al., 2018; Lamsal et al., 2015; Goldberg et al., 2021; Dressel et al., 2022;
93 Goldberg et al., 2024; Harkey & Holloway, 2024; Bechle et al., 2013; H. J. Lee et al., 2023; Xu
94 & Xiang, 2023). This study extends these prior assessments of NO₂ column-to-surface
95 agreement, where we focus on frequency distributions to capture the net impact of day-to-day
96 variability.

97 ~~Past studies comparing surface and satellite NO₂ have found temporal correlation of daily values~~
98 ~~at individual sites ranging from $r = 0.61$ to $r = 0.69$ (Lamsal et al., 2014; Lamsal et al., 2015),~~
99 ~~monthly and seasonal values at individual sites ranging from $r = 0.67$ to $r = 0.90$ (Griffin et al.,~~
100 ~~2019; Yu & Li, 2022; Harkey & Holloway, 2024; Dressel et al., 2022; Xu & Xiang, 2023;~~
101 ~~Lamsal et al., 2015), and annual average values at sites ranging from $r = 0.68$ to $r = 0.93$ (Zhang et~~
102 ~~al., 2018; Lamsal et al., 2015; Goldberg et al., 2021; Kim et al., 2024; Beechle et al., 2013; H. J.~~
103 ~~Lee et al., 2023). Here, r refers to the Pearson correlation coefficient, which measures the~~
104 ~~strength and direction of a linear relationship between variables. In some cases, these~~
105 ~~comparisons adjusted column values to the surface (e.g. Lamsal et al., 2014) and/or adjusted~~
106 ~~ground monitors to reduce the error in chemiluminescent detection of NO₂ (e.g. Lamsal et al.,~~
107 ~~2015; Beechle et al., 2013). Using similar methods, TROPOMI tends to show better agreement~~
108 ~~with annual AQS NO₂ than does OMI, e.g. $r = 0.81$ using TROPOMI (Goldberg et al., 2015)~~
109 ~~versus $r = 0.68$ from OMI (Lamsal et al., 2015). Off road AQS monitors tend to show better~~
110 ~~agreement with satellite data than near road AQS monitors, e.g. $r = 0.81$ – 0.87 at non near road~~
111 ~~sites versus $r = 0.64$ – 0.74 at near road sites (Kim et al., 2024). The underestimation of estimated~~
112 ~~near surface NO₂ near roads and localized sources is a recurring issue in OMI and TROPOMI~~
113 ~~NO₂ VCDs (Dressel et al., 2022; Goldberg et al., 2024; Ialongo et al., 2020).~~

114 The relationship between surface NO₂ and column abundance is influenced by physical and
115 chemical processes, many of which have seasonal components. In winter, shallow boundary
116 layers trap pollutants near the surface, leading to higher surface concentrations and increasing
117 surface-to-column agreement (Harkey et al., 2015). In summer, higher temperatures and

118 increased sunlight accelerate photochemical reactions, converting NO₂ into ozone and other
119 secondary pollutants, and decreasing surface-to-column agreement (Boersma et al., 2009).
120 Seasonal changes in emissions, such as high building-heating emissions in winter, and high
121 power plant emissions in summer (Frost et al., 2006; Levinson & Akbari, 2010) interact with
122 atmospheric processes causing an increase in NO₂ column abundance in winter in four-season
123 climates (Shah et al., 2020). Processes affecting the sources and sinks of NO₂ at the surface and
124 through the vertical column can also lead to temporal lags, with peak surface NO₂ preceding
125 peak column NO₂ in the mornings (Harkey et al. 2024).

126 Frequency distributions capture the variability, extremes, and patterns of pollutant abundance,
127 relevant to air quality standards, pollution trends, and the effectiveness of emission control
128 measures (Knox and Lange, 1974; Pollack, 1975; Venkatram, 1979; Chowdhury et al., 2021;
129 Mondal et al., 2021). For example, Mondal et al. (2021) used frequency distributions of ground-
130 based monitors to examine changes in air quality across Delhi and Kolkata during COVID-19
131 lockdown phases, showing how reduced human activity led to shifts in pollutant levels. We
132 extend this line of analysis by comparing NO₂ distributions across multiple dimensions with
133 TROPOMI and include time-of-day and resolution-dependence of results using data from
134 TEMPO, the Tropospheric Emissions: Monitoring of Pollution (TEMPO; Chance et al., 2019;
135 Neager et al., 2021; Zoggman et al., 2017). TEMPO provides daytime hourly observations of
136 NO₂ over North America and finer spatial coverage—approximately 2.1 km by 4.5 km at its
137 center.

138 The Jensen-Shannon Divergence (JSD) is a robust metric for comparing probability distributions
139 that is used within a wide variety of fields, including machine learning (Thiagarajan & Ghosh,
140 2024; Saurette et al., 2023; Tsigalou et al., 2021; Melville et al., 2005), data science (Toledo et
141 al., 2022; Zhao et al., 2024), biology (Yan et al., 2021; Jones et al., 2023; Ahmed et al., 2023),
142 and meteorology (Kibirige et al., 2023). In environmental research using satellite data, the JSD
143 has shown that the Mangrove Forest Index (MFI) from Sentinel-2 imagery outperforms
144 traditional vegetation indices in distinguishing submerged mangrove forests (Jia et al., 2019). In
145 air quality, JSD has been used to compare modeled and measured PM_{2.5} (Yang et al., 2024), and
146 to compare an air quality index (AQI) with measurements of specific air pollutants (Wang &

147 ~~Zhang, 2022). We utilize the JSD to quantify the similarity between satellite and monitored NO₂~~
148 ~~distributions, applying this well-established metric to satellite derived air quality evaluation.~~

149 In this work, we consider: (1) How do the distributions of satellite NO₂ VCD compare with those
150 for near-surface NO₂? (2) To what degree does new hourly data from TEMPO improve the
151 agreement between surface and space based NO₂ distributions? For both questions, we consider
152 spatial variability, especially proximity to roadways, and temporal variability including
153 seasonality and diurnal variability. By considering the ability of satellites to capture peak NO₂
154 values in a comparable distribution to surface data, we consider how satellite VCDs can support
155 air quality management, improve health impact analysis, and inform air pollution monitor siting.

156 **2 Data and Methods**

157 In this study, we evaluate the ability of two satellite instruments, TROPOMI and TEMPO, to
158 capture the spatial and temporal variability in NO₂ surface concentration distributions across the
159 continental United States (CONUS), as measured by AQS monitors. By comparing the
160 coefficient of variation (CV) and Jensen-Shannon divergence (JSD) between satellite and
161 monitor data, we aim to assess the alignment between the datasets.

162 **2.1 EPA Surface Monitor Data**

163 The EPA Air Quality System (AQS) contains hourly NO₂ measurements from ground-based
164 monitors, providing high temporal resolution data that are critical for assessing compliance with
165 the U.S. National Ambient Air Quality Standards (NAAQS). There are two NAAQS related to
166 NO₂: one for annual average concentration, set at 53 ppb, and one based on peak 1-hour
167 concentrations, set at 100 ppb, based on the 3-year average of the 98th percentile of the yearly
168 distribution of 1-hour daily maximum NO₂ concentrations (EPA, 2010). Enforcement of these
169 standards relies on data from AQS NO₂ monitors, a network that includes 431 monitors as of
170 August 2024. Because NO₂ has a relatively short atmospheric lifetime, typically ranging from a
171 few hours to a day depending on meteorological conditions (Lange et al., 2022; Liu et al., 2021),
172 ground monitors are expected to capture local conditions (Wang et al., 2020).

173 The EPA Air Quality System data (AQSEPA, 2025) was used to access NO₂ monitor data for the
174 years 2019 through 2023 from all available sites in CONUS during this time period (N=503
175 unique monitors from 2019 to 2023). We note that there are some areas that are overrepresented
176 by NO₂ monitors, and others that are lacking monitors. Specifically, most monitors are located in
177 urban areas, especially on the East Coast and in Southern California, meaning that rural areas
178 tend to be less represented by ground monitors. Most monitors use a chemiluminescence method,
179 where the amount of NO₂ that is converted to NO is measured by a molybdenum oxide converter
180 (Fontijn et al., 1970). The converter also reacts with other oxidized nitrogen compounds such as
181 nitric acid (HNO₃) and peroxyacetyl nitrate (PAN) to form NO (Dunlea et al., 2007; Steinbacher
182 et al., 2007), which can lead to an overestimation of NO₂. Corrections for this bias have been
183 applied when comparing with satellite observations (e.g. Cooper et al., 2020; Lamsal et al., 2015;
184 Li et al., 2021). Uncorrected AQS NO₂ has been used for determining compliance with the
185 NAAQS and for health assessments, which is the approach we take here, consistent with prior
186 studies focused on regulatory relevance (Novotny et al., 2011; Penn & Holloway, 2020; Harkey
187 and Holloway, 2024; Goldberg et al., 2021; Kim et al., 2024; Duncan et al., 2013; Qin et al.,
188 2019). More recently, some NO₂ monitors have been added to the network which measure “true
189 NO₂” using Cavity Attenuated Phase Shift Spectroscopy (CAPS, Kebabian et al., 2005). These
190 monitors are expected to be more representative of ground-level NO₂ concentrations and have
191 less overestimations since they directly measure NO₂ and no other species (Ge et al., 2013).
192 Some of the monitors used in this study use CAPS methodology to measure NO₂. We discuss the
193 comparison of CAPS versus traditional NO₂ monitors in results Sect. 3.1.

194 Hourly AQS measurements at 13:00 and 14:00 local time (LT) were averaged to align with the
195 TROPOMI overpass of ~13:30 LT. Hourly AQS measurements from 12:00 GMT to 23:00 GMT
196 are compared with hourly TEMPO data for daylight hours. For both the TROPOMI and TEMPO
197 analyses, AQS data are filtered to ensure consistency with satellite data availability. As a result
198 of filtering monitoring data for TROPOMI and TEMPO separately, the subsets of monitor data
199 available for comparison with each instrument differ, even for the same time periods.

200 **2.2 TROPOMI Data**

201 The Tropospheric Monitoring Instrument (TROPOMI; [European Space Agency, 2021](#)) is on
202 board the Copernicus Sentinel-5 Precursor satellite which has a daily, local overpass time of
203 ~13:30 LST (Veefkind et al., 2012). Currently, the highest resolution of TROPOMI is 3.5 km by
204 5.5 km at nadir which has increased from 3.5 km by 7.0 km since August 6th, 2019. Daily
205 TROPOMI NO₂ data for the years 2019 through 2023 were allocated to a 4 km x 4 km grid over
206 CONUS using the Wisconsin Horizontal Interpolation Program for Satellites (WHIPS; [Center](#)
207 [for Sustainability and the Global Environment, 2024](#); Harkey et al., 2015, 2021; Harkey and
208 Holloway, 2024; Penn and Holloway, 2020). Using WHIPS, we also remove data with quality
209 flag lower than 0.75. Each monitor location was compared with the 4 km x 4 km gridded
210 TROPOMI value in the corresponding grid cell. December 2023 and July 2024 4 km x 4 km
211 TROPOMI NO₂ data were also collected for each of the monitors for comparison with TEMPO
212 data.

213 [A 4 km x 4 km oversampled grid is used as opposed to the 1 km x 1 km oversampled grid since](#)
214 [this study focuses on daily observations, and the 1 km x 1 km grid is best suited for monthly or](#)
215 [annual averages \(Goldberg et al., 2021\). To ensure a valid number of TROPOMI pixels were](#)
216 [being represented despite the higher grid resolution, we analyzed the number of ground monitors](#)
217 [falling within each TROPOMI pixel by performing a spatial join between ground monitor](#)
218 [locations and the oversampled 4 km x 4 km TROPOMI grid. About 97% of TROPOMI pixels](#)
219 [contain only one monitor, with only a small number of pixels \(2.7%\) containing more than one.](#)
220 [Figure S1 shows the number of monitors per TROPOMI pixel \(locations where there are more](#)
221 [than 1 monitor per TROPOMI pixel\) and the number of valid TROPOMI retrievals from 2019 to](#)
222 [2023 at each grid cell, confirming that monitors are well-distributed enough to not](#)
223 [disproportionately cluster within a small subset of satellite pixels. Since monitors are spread](#)
224 [across the entire U.S. and most are at least 4 km apart, there is generally sufficient separation to](#)
225 [ensure that most monitors are assigned to distinct TROPOMI pixels rather than falling into the](#)
226 [same grid cells repeatedly.](#)

227 2.3 TEMPO Data

228 The TEMPO instrument launched onboard the Intelsat 40e mission (NASA, 2024), a
229 geostationary satellite, on April 7, 2023. TEMPO provides hourly measurements of atmospheric

230 pollutants over North America (Chance et al., 2019; Naeger et al., 2021; Zoogman et al., 2017).
231 TEMPO achieves a spatial resolution of approximately 2.1 km in the north-south direction and
232 4.5 km in the east-west direction at the center of its Field of Regard (FOR), centered around
233 36.5° N and 100° W (Chance et al., 2019). The TEMPO Level-3 (L3) NO₂ data (Suleiman, 2024)
234 used in this study were accessed through NASA's EarthData Search portal.

235 In order to synchronize TEMPO and ground-based hourly measurements, TEMPO timestamps
236 were rounded to the nearest hour, with mid-hour values rounded up. All files within each
237 rounded-hour group were averaged, producing a single NO₂ value per hour per day. Only
238 TEMPO observations with a main data quality flag of 0 and cloud fraction at or less than 0.2
239 were retained, in line with TEMPO documentation guidelines (NASA Langley Research Center,
240 2024).

241 For the comparison with TROPOMI, the UTC equivalents of 1 pm and 2 pm LT were
242 determined for each time zone based on the latitude and longitude of each monitor location.
243 TEMPO NO₂ values corresponding to these calculated UTC hours were averaged to align with
244 the TROPOMI overpass time (~13:30 LST). Similarly, for ground-based measurements, the
245 monitor data were filtered to include only values corresponding to 1 pm and 2 pm LT and then
246 averaged.

247 2.4 Monitor Classification

248 To classify the monitors by roadway proximity, the state-level Census Bureau's 2021
249 TIGER/Line shapefiles for Primary and Secondary Roads ([2021 TIGER/Line® Shapefiles](#),
250 [2025](#)) were combined to form a comprehensive dataset for the CONUS domain.

251 To evaluate how TROPOMI and ground-based monitor NO₂ values vary by proximity to a road,
252 monitors were also assigned to different groups based on their distance from a road (\leq 20-m, 20
253 to 50-m, 50 to 300-m, 300-m to 1 [kilometer](#), and >1 [kilometer](#)), where buffer distances are calculated
254 from the road shapefiles (Figure S32). There were 9 monitors that were 20 meters or less away
255 from a road, 66 between 20 and 50 meters from a road, 108 between 50 and 300 meters, [167219](#)
256 between 300 meters and 1 [kilometer](#), and [15304](#) that were greater than 1 [kilometer](#) from
257 a road.

258 Roads were also classified into three categories: (1) interstates, (2) highways, and (3) other
259 roads, based on their route type code (RTTYP) values. Where monitors are considered as
260 representing a roadway category, we followed the criteria of the EPA Near-Road-Network
261 (Gantt et al., 2021; Kim et al., 2024), to merge monitor locations with road buffers, considering
262 the 50-m buffer recommended by EPA, as well as a less restrictive 300-m buffer. In each case,
263 monitors inside the buffer of a particular roadway type were classified as representing that
264 category. If a monitor fell within multiple buffers, it was assigned the classification of the largest
265 road type. Monitors not falling within any buffers were classified as "non-roadway."

266 Using the 50-m buffer, 58 monitors were classified as "interstate," 17 as "highway," and 428 as
267 "non-roadway" (Figure S24; no monitors classified as "other roads"). Using the 300-m buffer, 91
268 monitors were classified as "interstate," 90 as "highway," 320 as "non-roadway," and 2 as "other
269 roads." Since there were no monitors classified as "other roads" for the 50-m buffer, this
270 category is excluded from the analysis.

271 We classified interstate monitors as urban or rural using the U.S. Census Bureau 2020 Urban
272 Areas Tiger/Line Shapefile (U.S. 2020 Urban Areas Shapefile, 2025). Only one interstate
273 monitor was identified as rural, so this analysis is not included.

274 **2.5 Data Analysis**

275 The frequency distribution of ambient pollutants in urban areas has long been recognized as a
276 useful metric for comparison with health-based thresholds, and to assess the effectiveness of
277 emission controls. Early studies found pollutant concentrations in urban areas to be
278 approximately lognormally distributed (Knox and Lange, 1974; Pollack, 1975; Venkatram,
279 1979) and isolated point sources better described by exponential distributions (Venkatram,
280 1979). The distributional lens also bears relevance to advanced health and regulatory assessment
281 (Chowdhury et al., 2021; Mondal et al., 2021). In this study we evaluate the capability of current-
282 generation satellites to capture the variability of near-surface nitrogen dioxide (NO₂) monitoring
283 data, with the goal of supporting health and regulatory applications.

284 The coefficient of variation (CV) was calculated for ground-level monitor data and for satellite
285 data. This metric was used to compare the relative variability of NO₂ between satellite and

286 ground-level data despite different measurement units (Aerts et al., 2015). CV is defined as the
287 ratio of the standard deviation (σ) to the mean (μ) of the data:

288

$$CV = \left(\frac{\sigma}{\mu} \right) \times 100$$

289 The Jensen-Shannon Divergence (JSD) is used to quantifyies the similarity between the
290 distributions of NO_2 from the satellite and ground-level monitors despite the different
291 measurement units (Menéndez et al., 1997). The Jensen-Shannon Divergence (JSD) is a robust
292 metric for comparing probability distributions that is used within a wide variety of fields,
293 including machine learning (Thiagarajan & Ghosh, 2024; Saurette et al., 2023; Tsigalou et
294 al., 2021; Melville et al., 2005), data science (Toledo et al., 2022; Zhao et al., 2024), biology
295 (Yan et al., 2021; Jones et al., 2023; Ahmed et al., 2023), and meteorology (Kibirige et al.,
296 2023). In environmental research using satellite data, the JSD has shown that the Mangrove
297 Forest Index (MFI) from Sentinel-2 imagery outperforms traditional vegetation indices in
298 distinguishing submerged mangrove forests (Jia et al., 2019). In air quality, JSD has been
299 used to compare modeled and measured $\text{PM}_{2.5}$ (Yang et al., 2024), and to compare an air
300 quality index (AQI) with measurements of specific air pollutants (Wang & Zhang, 2022). We
301 utilize the JSD to quantify the similarity between satellite and monitored NO_2 distributions,
302 applying this well-established metric to satellite-derived air quality evaluation.

303 To calculate the JSD, each dataset was binned, with a bin size of 1 ppb (for ground monitors) or
304 1×10^{15} molecules/cm² (for satellite data), ranging from 0 to 40 ppb or 40×10^{15} molecule/cm²,
305 with an additional bin for values exceeding 40 ppb or 40×10^{15} molecule/cm². For visualization
306 purposes, the frequency distributions are binned with the ground monitors ranging from 0 to 40
307 ppb and the satellite data ranging from 0 to 30×10^{15} molecule/cm², with an additional bin for
308 values exceeding 40 ppb or 30×10^{15} molecule/cm². Depending on the specific analysis, NO_2
309 data are grouped by: (1) Distance from roadways (in meters) – TROPOMI daily data from 2019
310 to 2023 (and corresponding ground monitors) are grouped by proximity to roads to assess spatial
311 alignment; (2) season – TROPOMI daily data from 2019 to 2023 (and corresponding ground
312 monitors) are grouped by season to analyze temporal alignment; (3) month – TROPOMI daily
313 data from December 2023 and July 2024, along with TEMPO and ground monitors at the

314 TROPOMI overpass time (~1:30 pm LT, represented by the average of 1 pm and 2 pm LT data),
315 are grouped by month to compare the temporal differences in alignment between TEMPO and
316 TROPOMI; and (4) road type (interstate, highway, non-roadway) – Both TROPOMI (daily),
317 TEMPO (calculated overpass time and hourly), and ground monitor data are grouped by road
318 type to evaluate varying alignment based on road classifications.

319 Binned data were then normalized to form probability distributions. The divergence was
320 calculated as:

321
$$JSD(P, Q) = \frac{1}{2} [D_{KL}(P||M) + D_{KL}(Q||M)]$$

322 where P and Q represent the probability distributions from the monitor and satellite data,
323 respectively, and M is the average of P and Q. The divergence D_{KL} is the Kullback-Leibler
324 divergence between each distribution and their mean (Clim et al., 2018). JSD values range from
325 0 to 1, with lower values indicating greater similarity between the satellite and monitor
326 distributions. In general, a $JSD < 0.1$ indicates very good alignment, $0.1 \leq JSD < 0.3$ indicates
327 moderate alignment, and $JSD \geq 0.3$ (Kibirige et al., 2023) indicates poor alignment.

328 **3 Results**

329 To evaluate the agreement between satellite and monitored NO_2 distributions, we consider the
330 impact of monitor location using TROPOMI; impact of season using TROPOMI; the comparison
331 of distributions between TROPOMI and TEMPO; and the impact of time-of-day using TEMPO.

332 **3.1 Alignment of TROPOMI NO_2 Distributions with Surface NO_2 Distributions**

333 This section analyzes TROPOMI and ground-based NO_2 measurements across varying distances
334 from roads, different seasons, and at monitors located near interstates, highways, and non-
335 roadway sites. Our results show that as the distance from roads increases, the distributions of
336 surface and column NO_2 become more similar. Monitor distributions near interstates and
337 highways exhibit lower agreement with TROPOMI distributions compared to those farther from
338 major roadways. Seasonally, alignment is strongest in winter and weakest in summer.

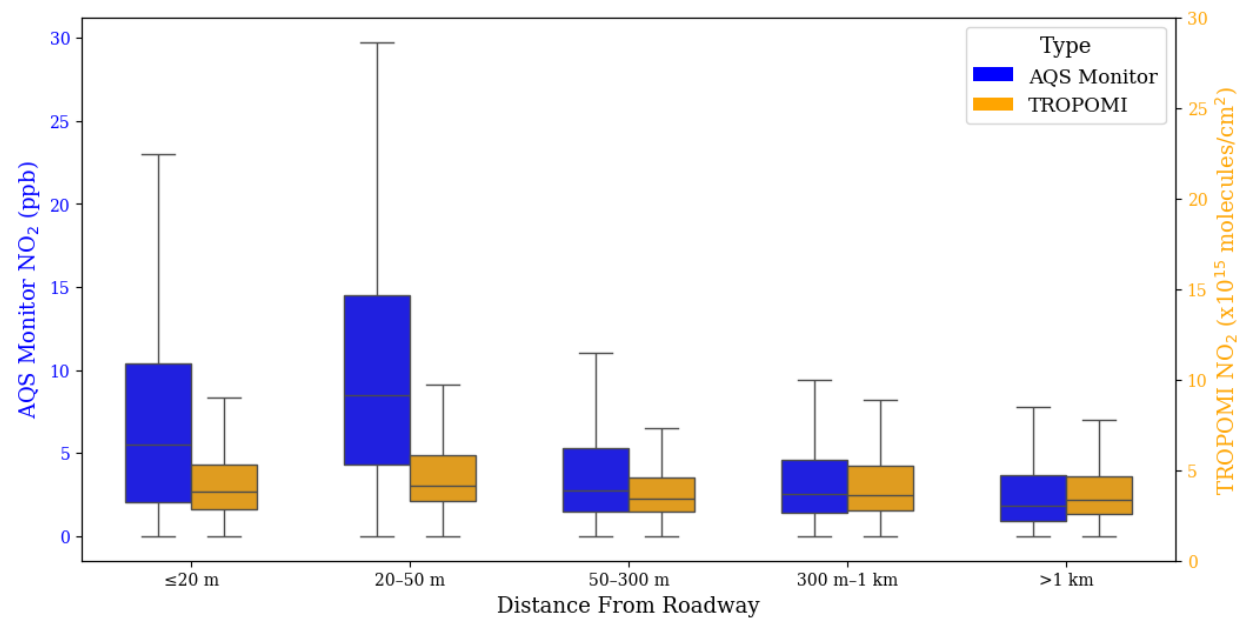
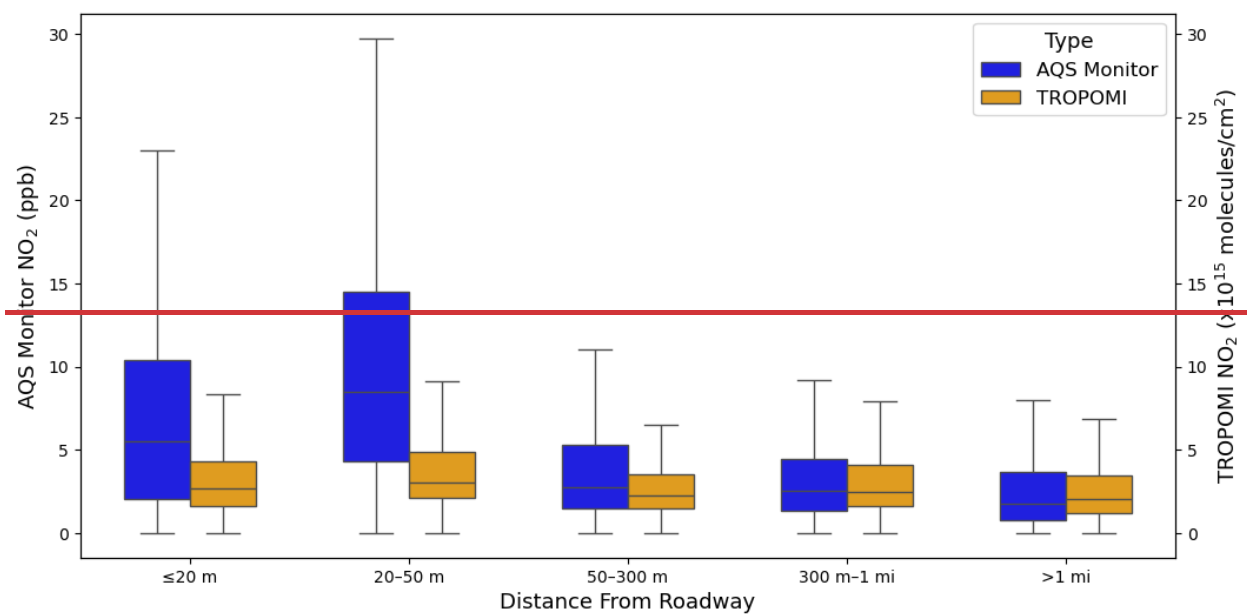
339 Figure 1 illustrates the distribution of NO₂ levels measured by AQS ground-based monitors and
340 TROPOMI observations as a function of distance from roadways using daily measurements from
341 2019 to 2023. For both data sources, mean, peak, and minimum NO₂ are all highest in the 20 –
342 50 m distance category (the second closest near-road category). NO₂ abundance decreases as
343 distance-to-road increases, and to a lesser extent as distance-to-road decreases. The somewhat
344 lower abundance \leq 20 m vs. the 20 – 50 m category may be due to the speciation of NO_x, where
345 NO is more abundant and converts to a higher fraction of NO₂ as distance-to-road increases
346 (Kimbrough et al., 2017). Most direct vehicle emissions are in the form of NO, and close to the
347 roadway, NO and NO₂ readily convert between forms. Limited ozone availability—especially
348 during stable conditions, which contribute to suppressed vertical mixing—can slow the
349 conversion of NO to NO₂ (Richmond-Bryant et al., 2017). As a result, NO₂ may initially be
350 suppressed very close to the road, and changes in total NO_x are primarily driven by mixing and
351 dilution rather than chemical transformation. Mean monitored NO₂ is 6.85 ppb at \leq 20 m, 10.47
352 ppb at 20 – 50 m, 4.53 ppb at 50 – 300 m, 3.7153 ppb at 300 m – 1 km^{mi}, and 2.8076 ppb at $>$ 1
353 km^{mi}. Mean TROPOMI NO₂ is 3.38×10^{15} molecules/cm² at \leq 20 m, 4.21×10^{15} molecules/cm² at
354 20 – 50 m, 3.00×10^{15} molecules/cm² at 50 – 300 m, 3.7263 $\times 10^{15}$ molecules/cm² at 300 m – 1
355 km^{mi}, and 3.1304×10^{15} molecules/cm² at $>$ 1 km^{mi}. Monitor values show a higher sensitivity
356 to roadway proximity, where the highest mean monitored concentration is 3759% of the lowest
357 mean concentration, compared to TROPOMI where the highest mean VCD is 14038% of the
358 lowest mean VCD.

359 Monitored NO₂ levels drop over 50% at \sim 50 m from the roadway (based on change in the mean,
360 upper 2.5 interquartile range, IQR, and the upper 1.5 IQR), a finding that compares with 31%
361 reduction in NO₂ between 20m and 300m from Kimbrough et al. (2017), as well as other studies
362 that identify a decrease in NO₂ at further distances (Karner et al., 2010; Richmond-Bryant et al.,
363 2017). TROPOMI VCDs also show the greatest change with roadway distance at \sim 50 km, but by
364 less than 30% (based on change in the mean, upper 2.5 IQR, and the upper 1.5 IQR).

365 Just as total NO₂ abundance, from both monitors and satellite, is highest at distances of 20-50 m
366 from the roadway, the range of daily values is also widest for the 20 – 50 m range and smallest at
367 the $>$ 1 km^{mi} range. Monitored values have a standard deviation of 8.24 ppb in the 20 – 50 m
368 range, and a standard deviation of 3.3944 ppb in the $>$ 1 km^{mi} range. The distribution of satellite

369 data does not vary as much in size across roadway locations, with a standard deviation of $3.90 \times$
370 10^{15} molecules/cm² for the 20 – 50 m range and 3.319×10^{15} molecules/cm² for the > 1 kmmile
371 range. In the 20 – 50 m range, the upper IQR of AQS NO₂ is 38% higher than the mean.
372 TROPOMI shows less variability than the monitors, with the 20 – 50 m upper IQR 16% higher
373 than the mean. As distance from the roadway increases, the distributions of data from ground and
374 satellite become more comparable. In the > 1 kmmile range, the upper IQR of monitor NO₂ is
375 2330% higher than the mean and the upper IQR of satellite data is 15% higher than the mean.
376 The ranges show more similarity at greater distance from the roadway, but even at distances of >
377 1 kmmile, the range of monitored values exceeds the range of satellite VCDs. These patterns
378 agree with Kim et al. (2024), who found that surface monitors show better agreement with
379 TROPOMI further from major roads. This improved alignment at greater distances likely reflects
380 the reduced influence of localized emission sources, which tend to create sharp gradients and
381 rapid variability near roads. In areas further from traffic, NO₂ concentrations vary more gradually
382 or are generally more uniform. As a result, surface monitors away from roads reflect broader
383 conditions, in better agreement with the coarser spatial resolution of TROPOMI.

384 When analyzed by season (Figure S4), the relationships are similar, except winter shows the
385 highest IQRs with the 20 to 50 m distance group having an IQR of 11.40 ppb for monitors and
386 4.96×10^{15} molecules/cm² for TROPOMI, and summer the lowest IQRs for both monitors (IQR
387 = 9.05 ppb) and TROPOMI (IQR = 1.71×10^{15} molecules/cm²). In the greater than 1 km distance
388 group, again winter has the highest IQRs (monitor IQR = 4.60 ppb; TROPOMI IQR = $3.95 \times$
389 10^{15} molecules/cm²) and summer the lowest IQRs (monitor IQR = 2.05 ppb; TROPOMI IQR =
390 1.55×10^{15} molecules/cm²).



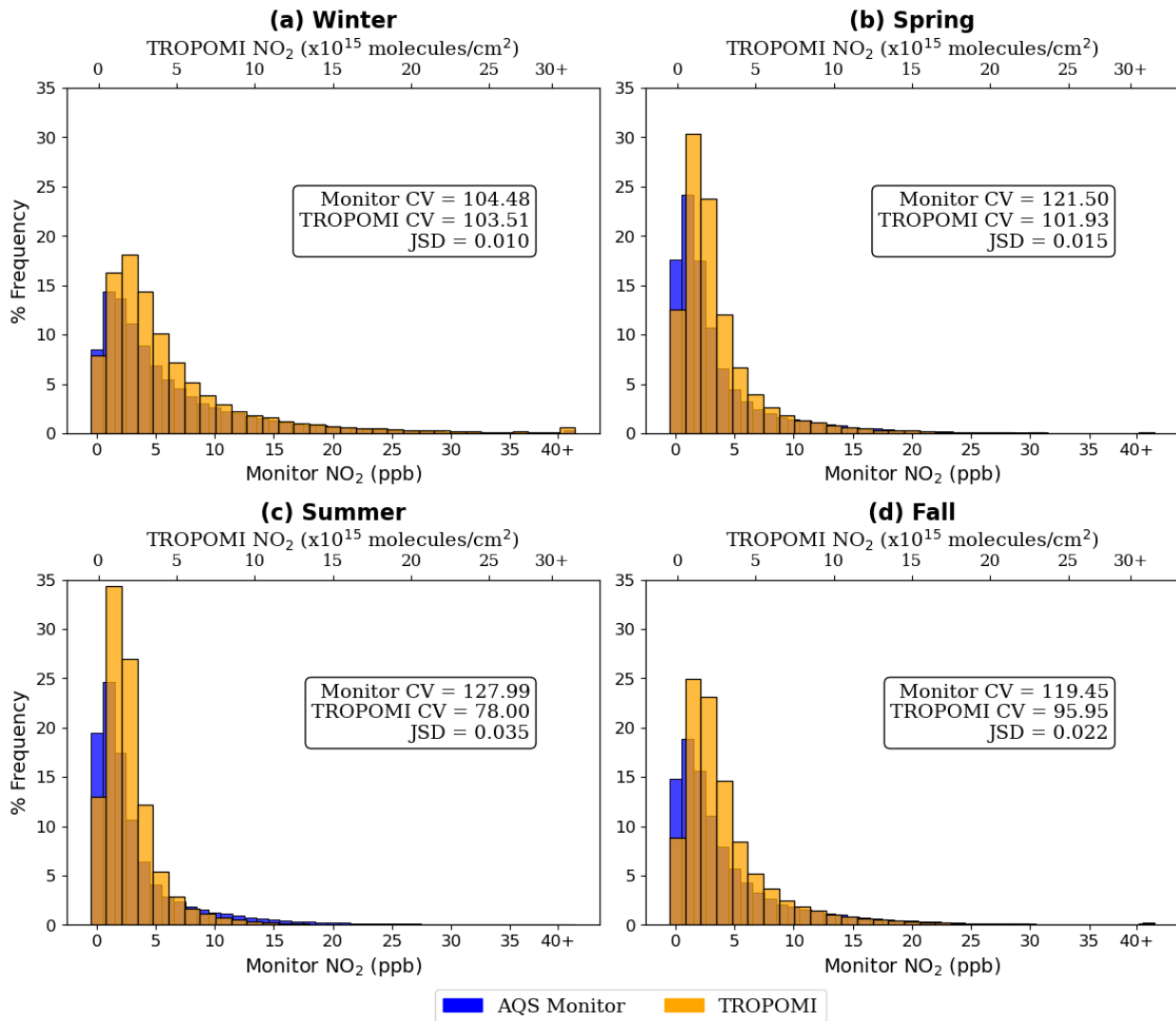
393 Figure 1. Box plots show median and interquartile ranges of all daily 2019 to 2023 NO₂ as
 394 measured by AQS monitors (blue) and TROPOMI (orange) across various distances from
 395 roadways, with the whiskers extending to the 1.5 IQR range. No outliers are shown. The left y-
 396 axis represents AQS monitor values in parts per billion (ppb), and the right y-axis represents
 397 TROPOMI NO₂ values in 10^{15} molecules per cm². The distance categories from the roadway
 398 include ≤ 20 m, 20-50m, 50-300m, 300m-1km, and > 1 km.

400 To consider the shape of monitored and satellite NO₂ distributions, we consider the effect of
401 season in Fig. 2. The winter distributions (Figure 2a, calculated from December, January, and
402 February data) exhibit the longest tails and highest NO₂ values. In winter the 90th percentile of
403 monitoring data is 14.80 ppb and the 90th percentile of TROPOMI data is 10.93×10^{15}
404 molecules/cm². Spring distributions (Figure 2b; March, April, and May) show intermediate
405 behavior, with lower values and shorter tails than winter and fall, but higher than summer (90th
406 percentile from monitors = 9.71 ppb; 90th percentile from TROPOMI = 6.19×10^{15}
407 molecules/cm²). In summer (Figure 2c, June, July, and August) the distributions exhibit the
408 shortest tails, and the lowest NO₂ values (90th percentile from monitors = 9.00 ppb, 90th
409 percentile from TROPOMI = 4.57×10^{15} molecules/cm²). Fall (Figure 2d; September, October,
410 and November) also shows intermediate behavior, generally between winter and spring (90th
411 percentile from monitors = 12.15 ppb; 90th percentile from TROPOMI = 7.44×10^{15}
412 molecules/cm²). The fall (Figure 2d, September, October, and November) and spring (Figure 2b,
413 March, April, and May) distributions show behavior in between winter and summer. The higher
414 NO₂ values in winter from monitor and TROPOMI data are attributed to reduced photochemical
415 activity in winter leading to longer NO₂ lifetimes (Harkey et al., 2015; Boersma et al., 2009;
416 Shah et al., 2020).

417 The highest percent frequencies for the monitor and TROPOMI distributions generally occur
418 within the 1–2 ppb or $1–2 \times 10^{15}$ molecules/cm² bin. However, the winter TROPOMI distribution
419 peaks in the $2–3 \times 10^{15}$ molecules/cm² bin with a percent frequency of 18.14%, compared with
420 winter monitor highest frequency of 14.33%. The highest percent frequency in spring from
421 TROPOMI is 30.39% versus monitor 24.15%; in summer TROPOMI is 34.35% versus monitor
422 of 24.68%; in fall TROPOMI is 24.90% versus monitor of 18.89%. These results indicate that
423 TROPOMI consistently records higher peak frequencies than the monitors, whereas monitors
424 consistently show a wider distribution.

425 Figure 2 provides a seasonal breakdown of the coefficient of variation (CV) and Jensen-Shannon
426 divergence (JSD) for both monitor and TROPOMI data across all monitors. Summer exhibits the
427 highest variability in monitored NO₂ concentrations (CV = 127.99%), but the lowest variability
428 in satellite observations (CV = 78.00%). The highest variability in TROPOMI occurs in winter
429 (CV = 103.51%), similar to the variability from monitor data (CV = 104.48%). Satellite CVs

430 generally follow a similar pattern to that of the monitors, though the overall variability is lower
 431 for satellite data across seasons.



432

433 Figure 2. Seasonal frequency distributions of 2019-2023 NO_2 as measured by AQS ground-based
 434 monitors (blue) and TROPOMI (light orange) data for four seasons: a) winter, b) spring, c)
 435 summer, and c) fall. The x-axes indicate the range of NO_2 , with the primary, lower x-axis
 436 showing monitor NO_2 concentrations in parts per billion (ppb) and the secondary, upper x-axis
 437 showing TROPOMI NO_2 VCD in 10^{15} molecules per cm 2 . The boxes show the Coefficient of
 438 Variation (CV; %) and Jensen Shannon Divergence (JSD) for each season.

439 This reduced variability in satellite observations can likely be attributed to the vertical mixing
 440 reflected in satellite retrievals, as well as horizontal spatial averaging reflected in satellite data

versus point-based NO₂ that are captured by ground monitors. This finding is consistent with previous studies that highlight the spatial averaging nature of satellite-based measurements, which integrate NO₂ amounts over a larger area than the point-based monitors (Ialongo et al., 2020).

Across all seasons shown in Fig. 2, JSD values are all low (< 0.1), indicating that TROPOMI may be good at predicting surface NO₂ across seasons. The alignment is strongest in winter (JSD = 0.010), while the divergence is highest in summer (JSD = 0.035), meaning the monitors and TROPOMI align best when the NO₂ lifetime is long in the colder months, and align the worst when the NO₂ lifetime is short in the warmer months. The better alignment in winter could also be attributed to winter having the largest range of values in the data, which reduces the sensitivity of the JSD calculation to small differences in the distributions. A wider spread in NO₂ values means that relative discrepancies between TROPOMI and monitor measurements are smaller in proportion to the total variability, potentially leading to greater similarity.

Across seasons, we find that CAPS or “true NO₂” monitors tend to have slightly worse alignment with TROPOMI than traditional, chemiluminescence monitors. Out of the monitors used in this study, 102 were identified as CAPS monitors, and 401 as traditional monitors. In winter, CAPS monitors have a JSD of 0.027 and traditional monitors a JSD of 0.009. In summer, CAPS monitors have a JSD of 0.078 and traditional monitors a JSD of 0.03. With all seasons combined, CAPS monitors have a JSD of 0.047 and traditional monitors have a JSD of 0.016.

Table 1 shows the CV and JSD for both monitor and satellite data from 2019 through 2023, aggregated across all seasons and separated by monitor classification (interstate, highway, and non-roadway), where roadway monitors are classified as being within 50 meters (Table 1a) or 300 meters (Table 1b) of a road. For the 50-m buffer (Table 1a), the coefficient of variation for ground-based monitor data increases progressively from interstate monitor locations to non-roadway locations, with interstate monitors exhibiting the lowest variability (CV = 75.07%) and non-roadway monitors showing the highest variability (CV = 118.17%). This indicates that NO₂ concentrations measured by ground monitors in interstate areas are more consistent compared to non-roadway regions. This pattern is mirrored in the satellite data, with CV values ranging from 91.62% for highway monitors to 106.16% for non-roadway monitors. These patterns suggest that

470 regular emissions play a larger role in determining near-road NO₂, where non-road areas vary
 471 with changes in wind patterns and the chemical environment.

472 For highway monitors, the CVs of satellite (CV = 91.62%) and monitor data (CV = 96.27%) are
 473 similar, indicating that TROPOMI performs similarly to ground monitors in capturing NO₂
 474 variability along highways. Near interstates, TROPOMI (CV = 92.60%) may capture more
 475 variability than the ground-based measurements (CV = 75.07%), a finding that contrasts with
 476 Fig. 1, where TROPOMI shows a narrower range of NO₂ values across all distances. This
 477 difference could stem from the fact that the interquartile ranges in Fig. 1 measure the spread of
 478 absolute values, while the coefficient of variation accounts for variability relative to the mean.
 479 Together, these metrics reveal that TROPOMI may not fully capture localized extremes
 480 (narrower IQR) but still captures more relative variability in pollution near interstates than
 481 monitors (higher CV).

	Road Type	Monitor CV	TROPOMI CV	JSD	# of Monitors
a) 50-m Buffer	Interstate	75.07	92.60	0.158	58
	Highway	96.27	91.61	0.095	17
	Non-roadway	118.17	106.16	0.009	428
b) 300-m Buffer	Interstate	77.20	91.014	0.133	91
	Highway	135.76	92.31	0.017	90
	Non-roadway	116.23	108.43	0.008	320

482

483 Table 1. Coefficient of variation ([%]) and Jensen-Shannon divergence for all seasons combined at
 484 interstate, highway, and non-roadway monitors 2019-2023 for the 50-m and 300-m roadway
 485 buffers.

486 The key differences seen within the JSD across the three monitor classifications are also present
 487 in the percent frequency distributions of NO₂ measured by ground-based monitors and
 488 TROPOMI (Figure S53), with interstate monitors having the lowest alignment (JSD = 0.158),
 489 highway monitors having better alignment (JSD = 0.095), and non-roadway monitors having the
 490 best alignment (JSD = 0.009). The strong alignment between TROPOMI and monitor
 491 distributions in non-roadway regions is consistent with previous studies (Dressel et al., 2022;
 492 Kim et al., 2024; Ialongo et al., 2020). This close alignment may be due to the relatively lower

493 NO₂ concentrations, which TROPOMI captures more accurately compared to regions with
494 higher emissions. These findings further align with previous work showing that TROPOMI tends
495 to underestimate NO₂ in high-pollution areas (such as interstates and highways) but slightly
496 overestimates in areas of lower pollution, such as rural areas (Dressel et al., 2022; Ialongo et al.,
497 2020; Goldberg et al., 2024).

498 Due to the large jump in NO₂ levels seen within Fig. 1 in the 50-300m category, we compare the
499 50-meter buffer roadway classifications (Figure S₅₃; Table 1a) with the 300-meter buffer
500 classifications (Figure S₆₄; Table 1b). Notable differences emerge between distributions,
501 particularly in the highway category, where 73 monitors are added to the highway distribution
502 (increasing from 17 to 90 monitors; Table 1) due to the larger buffer. The alignment between
503 monitor data and TROPOMI observations is significantly improved within the 300-meter buffer
504 near highways. This improvement in alignment is likely due to the decay of NO₂ with increasing
505 distance from the road (Karner et al., 2010; Kimbrough et al., 2017; Richmond-Bryant et al.,
506 2017). Consequently, the lower surface NO₂ concentrations observed at 300 meters are better
507 captured by TROPOMI. This is reflected in Table 12, which shows a substantial reduction in the
508 JSD for highway monitors, from 0.095 in the 50-meter buffer to 0.017 in the 300-meter buffer
509 (an 82% increase in alignment at the 300-meter buffer).

510 The differences observed in the highway category with the 300-meter buffer may be present
511 since the distribution includes 73 more monitors than the 50-meter buffer, capturing lower NO₂
512 amounts that are more aligned with TROPOMI's observations. On the other hand, the interstates
513 category exhibits less noticeable change, with only 33 additional monitors in the 300-meter
514 buffer distribution (increasing from 58 in the 50-meter buffer, Table 1a; to 91 in the 300-meter
515 buffer, Table 1b). This suggests that the monitors added in the 300-meter buffer for interstates
516 measure NO₂ levels similar to those already captured in the 50-meter buffer, resulting in little
517 change to the overall distribution.

518 These results indicate that TROPOMI follows the trend of NO₂ decreasing with increasing
519 distance from roadways that ground-based monitors record, and TROPOMI captures surface
520 concentrations best in winter and at 300+ meters away from the traffic source.

521

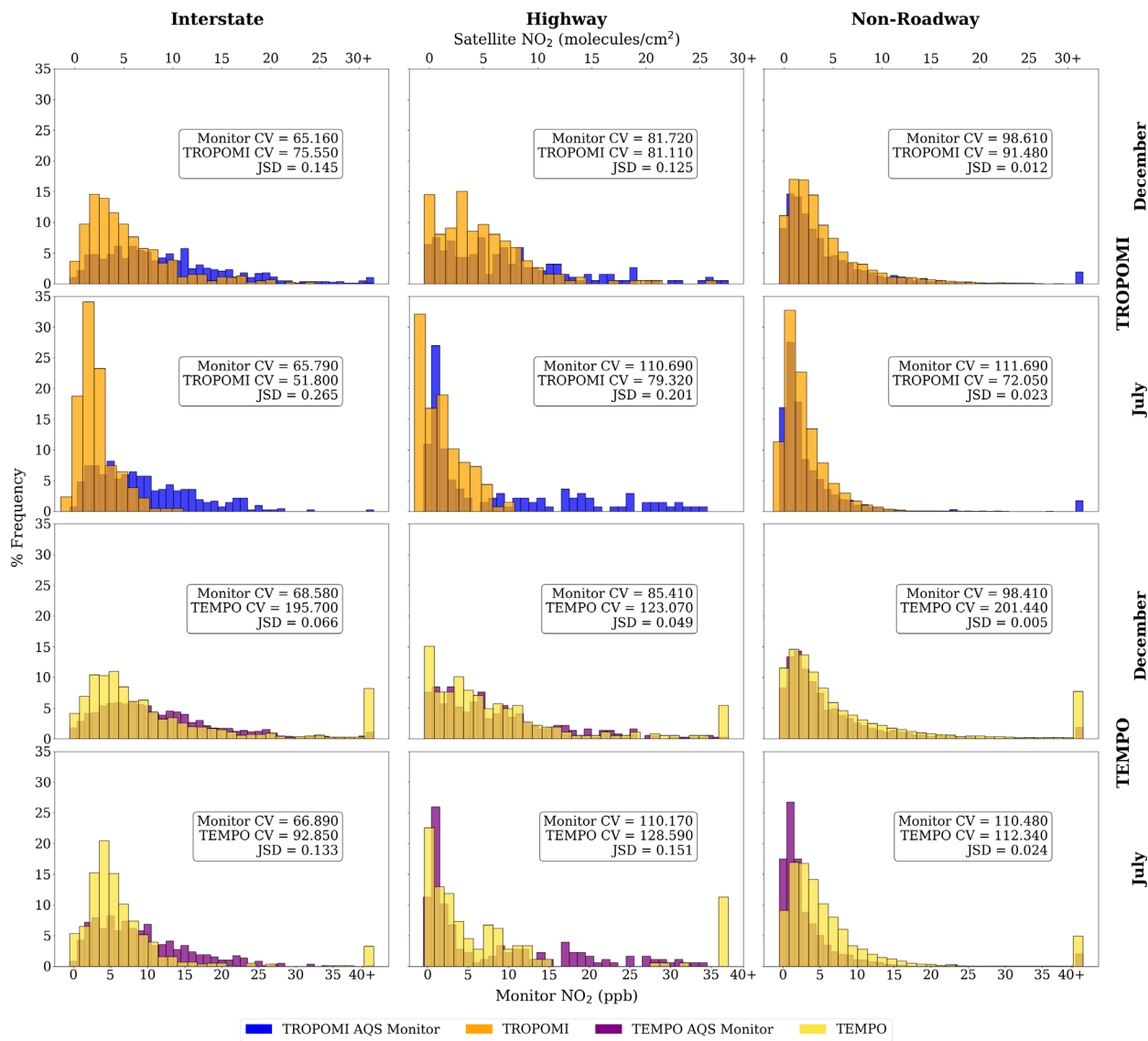
522 **3.2 Column-Column Daily Alignment**

523 Here we compare the distributions of NO₂ from TROPOMI and TEMPO with ground-based
524 monitors to assess how well each satellite instrument captures daily variations in NO₂
525 concentrations. Our results indicate that TEMPO consistently aligns more closely with ground-
526 based measurements than TROPOMI, particularly in high NO₂ areas such as highways and
527 interstates.

528 Figure 3 shows the distributions of NO₂ as measured by AQS ground-based monitors (filtered to
529 match valid TROPOMI and TEMPO data), TROPOMI, and TEMPO, separated by road
530 classifications (interstates, highways, and non-roadways) for December 2023 and July 2024. The
531 1 pm and 2 pm UTC (based on time zone) TEMPO and AQS values were averaged to align with
532 the TROPOMI overpass time of ~1:30 LT (see Sect. 2.3). The monitor data in each comparison
533 differs due to the data filtering (see Sect. 2.2 and 2.3). The comparison of frequency distributions
534 reveals how well TEMPO and TROPOMI capture the wide range of ground-based monitor
535 readings across these classifications and time periods.

536 In December 2023, TEMPO (JSD = 0.007) and TROPOMI (JSD = 0.021) exhibit across road
537 classifications show distinct patterns differences in how well they capture their ability to
538 represent NO₂ distributions across the various road classifications. Near interstates TEMPO
539 shows a 90th percentile at 18.34×10^{15} molecules/cm² where the TROPOMI 90th percentile is
540 11.27×10^{15} molecules/cm². TEMPO aligns more closely with monitor distributions with a JSD
541 of 0.066 compared to the TROPOMI JSD of 0.145 (Figure 3). TEMPO has 21.42% of data
542 points above 11×10^{15} molecules/cm² for interstate values in December, whereas TROPOMI
543 appears to underestimate the frequency of higher NO₂ levels more, with a cumulative frequency
544 of 10.53% above that threshold. Near highways, the TEMPO 90th percentile is 14.70×10^{15}
545 molecules/cm² compared to TROPOMI with a 90th percentile of 10.06×10^{15} molecules/cm². The
546 JSD for TEMPO is 0.049 and TROPOMI is 0.125 for highway monitors, indicating that TEMPO
547 has much better alignment on highways (Figure 3). For non-roadway locations, both instruments
548 show very good alignment (TEMPO JSD = 0.005; TROPOMI JSD = 0.012; Figure 3) with the
549 monitor data distributions, but with TEMPO again being slightly better.

550 In July 2024, the patterns show greater divergence across road classifications (TEMPO JSD =
551 0.027; TROPOMI JSD = 0.049) between the satellite observations and ground-based monitor
552 data compared to the December 2023 distributions. Near interstates, the TEMPO 90th percentile
553 is 8.46×10^{15} molecules/cm² and the TROPOMI 90th percentile is 5.58×10^{15} molecules/cm²,
554 with TEMPO aligning more closely (JSD of 0.133 compared to TROPOMI JSD of 0.265; Figure
555 3). TEMPO has 17.01% of data points above 7×10^{15} molecules/cm² for interstate values in July,
556 whereas TROPOMI appears to underestimate the frequency of higher NO₂ levels more, with a
557 cumulative frequency of 3.61% above that threshold. Near highways, TEMPO achieves a much
558 better representation of the higher observed NO₂ with a 90th percentile of 9.34×10^{15}
559 molecules/cm² compared to TROPOMI with a 90th percentile of 5.32×10^{15} molecules/cm². The
560 JSD for TEMPO is 0.151 and TROPOMI is 0.201 for highway monitors, indicating that TEMPO
561 has better alignment near highways. For non-roadway locations, both instruments show very
562 good alignment (TEMPO JSD = 0.024; TROPOMI JSD = 0.023; Figure 3) with the monitor data
563 distributions, with TEMPO and TROPOMI alignment with ground monitors being more
564 comparable than in December 2023.



565

566 Figure 3. December 2023 and July 2024 [at the TROPOMI overpass time \(~13:30 LST\)](#)
 567 frequency distributions of NO₂ as measured by AQS ground-based monitors filtered to the valid
 568 TROPOMI (blue) and TEMPO (purple), TROPOMI (light orange), and TEMPO (yellow) data
 569 for three monitor classifications: Interstate, Highway, and Non-roadway. The x-axes indicate the
 570 range of NO₂, with the primary, lower x-axis showing monitor NO₂ concentrations in parts per
 571 billion (ppb) and the secondary, upper x-axis showing TROPOMI NO₂ VCD and TEMPO NO₂
 572 VCD in 10¹⁵ molecules per cm². The boxes show the Coefficient of Variation (CV) and Jensen
 573 Shannon Divergence (JSD) for each season and monitor classification.

574 Throughout both December 2023 and July 2024, TEMPO's improved alignment with ground-
575 based monitors compared to TROPOMI may be attributed to several factors. TEMPO operates
576 from a geostationary orbit, allowing it to take hourly measurements and capture the diurnal
577 variability of NO₂ concentrations more effectively than TROPOMI, which has a single daily
578 overpass time. This high temporal resolution enables TEMPO to better match the timing of NO₂
579 peaks and fluctuations detected by ground-based monitors, which are also recorded on an hourly
580 basis. Additionally, TEMPO's finer spatial resolution, approximately 2 km in the north-south
581 direction and 4.5 km in the east-west direction, may allow it to capture more localized pollution
582 sources, such as traffic emissions along highways and interstates. This may be why we see such a
583 large difference in alignment in the interstate and highway categories between TEMPO and
584 TROPOMI, and very little difference in alignment in the non-road category. In contrast,
585 TROPOMI's 4 km x 4 km (re-gridded) resolution and single overpass time may be less effective
586 at capturing these localized variations. TEMPO's finer resolution in one direction and its frequent
587 observations may enable it to more precisely match the spatial and temporal variability detected
588 by ground-based monitors. The consistency of slight underestimation for both instruments in
589 high-pollution areas like highways and interstates suggests challenges in fully capturing elevated
590 NO₂ levels that occur near traffic sources. Overall, this indicates that while TEMPO generally
591 provides a closer approximation of NO₂ distributions compared to TROPOMI, both satellite
592 instruments show limitations, particularly in representing peak concentrations at high-polluting
593 sites.

594

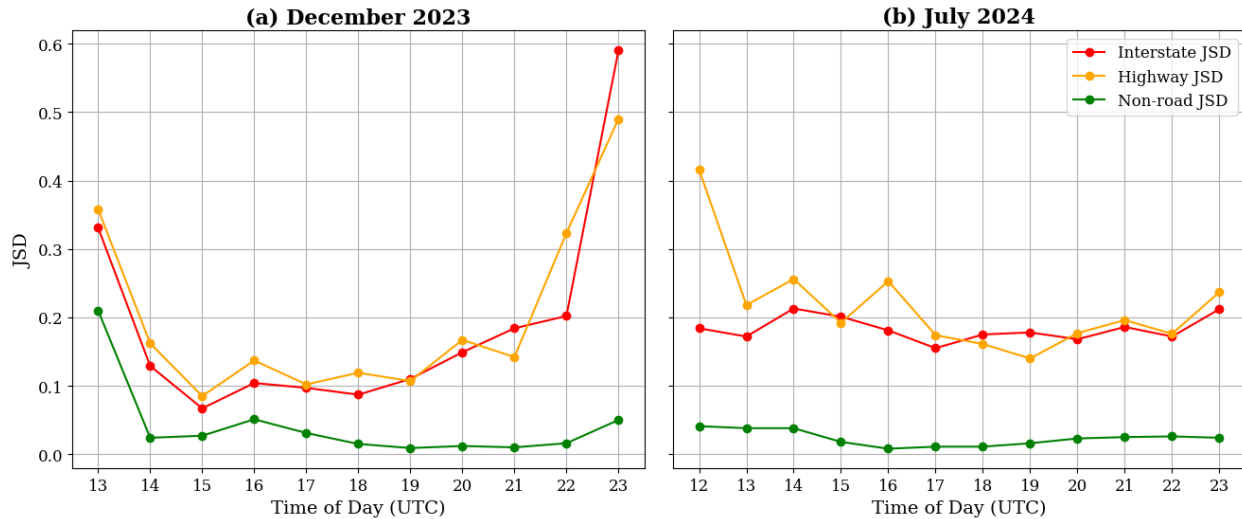
595 **3.3 Column-Surface Diurnal Alignment**

596 In this section we explore the hourly alignment among monitor observations and hourly TEMPO
597 observationsdistributions at interstate, highway, and non-roadway monitors. We find that
598 TEMPO aligns best with ground monitors around midday and exhibits poorer alignment in the
599 early morning and early evening.

600 Figure 4 presents the hourly JSD for TEMPO NO₂ measurements compared with ground
601 monitors categorized by interstate (red), highway (orange), and non-roadway (green) monitors
602 for December 2023 (Figure 4a) and July 2024 (Figure 4b). The results highlight distinct diurnal

603 patterns across road types and seasons, reflecting the influence of traffic emissions, atmospheric
604 mixing, and insulation.

605 In December 2023, all monitor categories exhibit similar trends in the early morning, with high
606 JSD values (highway JSD = 0.358; interstate JSD = 0.331; non-road JSD = 0.210) indicative of
607 moderate to poor alignment between TEMPO and ground-based monitors. This pattern,
608 consistent with early morning rush hour emissions and limited atmospheric vertical mixing
609 (Harkey and Holloway, 2024) as well as a decrease in TEMPO's measurement accuracy due to
610 high solar zenith angles in the morning according to TEMPO documentation (NASA Langley
611 Research Center, 2024), suggests that TEMPO may not capture rapid increases in NO₂ during
612 high traffic and low mixing periods. By mid-morning, JSD has decreased for all road types
613 (highway JSD = 0.085; interstate JSD = 0.067; non-road JSD = 0.027), indicative of good
614 alignment, with non-road monitors showing the most significant improvement (87% increase in
615 alignment). This pattern of better alignment in non-road monitor areas could be attributed to
616 lower NO₂ levels away from major sources of emissions. As the day progresses in December,
617 JSD values for highway and interstate monitors increase steadily (with highways fluctuating
618 more) after 17 UTC (~12 pm LT), with highways increasing in JSD from 0.102 to 0.490 and
619 interstates increasing from JSD 0.097 to 0.590, indicating worsening alignment in the afternoon
620 and early evening. This pattern may reflect the re-accumulation of NO₂ due to afternoon traffic
621 and the collapse of the boundary layer later in the afternoon (Harkey and Holloway, 2024), as
622 well as the decrease in TEMPO's measurement accuracy in the evening (NASA Langley
623 Research Center, 2024). Non-road monitors show less change in JSD through the day, suggesting
624 that TEMPO alignment is more consistent in non-road monitor areas throughout the rest of the
625 day, only fluctuating in JSD values between 0.009 and 0.05.



626

627 Figure 4. The a) December 2023 and b) July 2024 hourly (UTC) TEMPO NO₂ Jensen-Shannon
628 Divergences at interstate (red), highway (orange), and non-roadway (green) monitor locations.

629 In July 2024 highway and interstate monitors do not exhibit a clear diurnal pattern, with JSD
630 values fluctuating between 0.14 and 0.416 for highways and 0.155 and 0.212 for interstates
631 throughout the day. Consistent, localized traffic emissions and the shorter NO₂ lifetime during
632 the summer suggest a less variable distribution of NO₂. Non-road monitors in July show
633 somewhat worse alignment in the morning (JSD = 0.041), with improved agreement during the
634 late morning and early afternoon (JSD ranging between 0.008 and 0.025). The non-road JSD
635 remains fairly constant into the early evening, with alignment decreasing by about 13%,
636 indicating that sunlight may play a larger role in the alignment in the evening since the sun is at a
637 higher position in the sky during this time in the summer than in the winter (which increases in
638 JSD at this time), enhancing TEMPO's measurement accuracy in the early evening in July.

639 Both months exhibit their highest JSDs, and worst alignment, in the early morning or early
640 evening hours, which coincides with peak traffic times and the most uncertainty in TEMPO
641 observations caused by the solar zenith angle. The best alignment and lowest JSDs occur
642 sometime near midday (~10am LT to ~2pm LT).

643 The disparity between highways and interstates in TEMPO, where highways generally have the
644 highest JSD, differs from the pattern seen with TROPOMI, where interstates tended to
645 consistently exhibit worse alignment. This suggests that TEMPO's higher spatial and temporal

646 resolution may capture localized sources more effectively, leading to variations in alignment
647 based on the distribution and intensity of NO₂ sources.

648 **4 Conclusions**

649 This study evaluates the distributional alignment between satellite-derived NO₂ data from
650 TROPOMI, TEMPO, and ground-based AQS monitors across the U.S. Our findings highlight
651 several key points that inform the potential of satellite data for both regulatory and public health
652 applications, particularly in informing future NO₂ monitor siting strategies. Several limitations
653 and sources of uncertainty should be considered. Several limitations of this analysis include: (1)
654 The overrepresentation of AQS monitors in urban areas; (2) the temporal mismatch between
655 satellite and ground measurements; and (3) the distance from roads analysis doesn't consider
656 other local factors. A key limitation is the overrepresentation of urban areas in the AQS
657 monitoring network, which may bias our results toward urban areas. Since AQS monitors are
658 more densely located in urban regions with high emissions and complex local sources, the results
659 may not fully capture alignment in more rural areas with fewer monitoring stations. Another
660 important consideration is the slight temporal mismatch between satellite and ground-based
661 measurements. TROPOMI provides a single daily observation around 13:30 pm local solar time,
662 whereas ground monitors and TEMPO record NO₂ concentrations throughout the day. To better
663 align with TROPOMI's overpass, we averaged 1 pm and 2 pm LT TEMPO and ground monitor
664 NO₂ values. Since NO₂ concentrations can change rapidly due to meteorological conditions and
665 emissions variability, this averaging approach may introduce some error in comparisons between
666 TEMPO, TROPOMI, and ground-based measurements. The classification of monitors by
667 distance from roads is based on buffer analysis, which does not account for local factors such as
668 wind direction, terrain, proximity to industry, and traffic density, all of which influence NO₂
669 dispersion. Despite these uncertainties, our findings highlight patterns in column-surface NO₂
670 agreement and demonstrate the potential for satellite data to complement ground-based
671 monitoring.

672 The Jensen-Shannon Divergence (JSD) proved to be an essential tool in this study, offering a
673 robust and interpretable metric for comparing the alignment and similarity of NO₂ distributions.
674 Its symmetry and bounded range allowed us to evaluate the degree of similarity between satellite

675 and monitor NO_2 values across different spatial and temporal scales, providing a clear
676 quantitative framework for assessing the similarity of two different instruments.

677 Past studies comparing surface and satellite NO_2 have found temporal correlation of daily values
678 at individual sites ranging from $r=0.61$ to $r=0.69$ (Lamsal et al., 2014; Lamsal et al., 2015),
679 monthly and seasonal values at individual sites ranging from $r=0.67$ to $r=0.90$ (Griffin et al.,
680 2019; Yu & Li, 2022; Harkey & Holloway, 2024; Dressel et al., 2022; Xu & Xiang, 2023;
681 Lamsal et al., 2015), and annual average values at sites ranging from $r=0.68$ to $r=0.93$ (Zhang et
682 al., 2018; Lamsal et al., 2015; Goldberg et al., 2021; Kim et al., 2024; Bechle et al., 2013; H. J.
683 Lee et al., 2023). Here, r refers to the Pearson correlation coefficient, which measures the
684 strength and direction of a linear relationship between variables. In some cases, these
685 comparisons adjusted column values to the surface (e.g. Lamsal et al., 2014) and/or adjusted
686 ground-monitors to reduce the error in chemiluminescent detection of NO_2 (e.g. Lamsal et al.,
687 2015; Bechle et al., 2013). Using similar methods, TROPOMI tends to show better agreement
688 with annual AQS NO_2 than does OMI, e.g. $r=0.81$ using TROPOMI (Goldberg et al., 2015)
689 versus $r=0.68$ from OMI (Lamsal et al., 2015). Off-road AQS monitors tend to show better
690 agreement with satellite data than near-road AQS monitors, e.g. $r = 0.81-0.87$ at non-near-road
691 sites versus $r = 0.64-0.74$ at near-road sites (Kim et al., 2024). The underestimation of estimated
692 near-surface NO_2 near roads and localized sources is a recurring issue in OMI and TROPOMI
693 NO_2 VCDs (Dressel et al., 2022; Goldberg et al., 2024; Ialongo et al., 2020).

694

695 In this study, we find a pattern of decreasing NO_2 with increasing distance from traffic sources,
696 which is consistent with the findings of previous studies (Kimbrough et al., 2017; Karner et al.,
697 2010; Richmond-Bryant et al., 2017). While ground-based monitors and TROPOMI satellite data
698 may differ with proximity to roadways, particularly within 50-m, their measurements still follow
699 the same overall trend. This convergence with increasing distance may be due to the reduction of
700 localized near-road emissions and the broader atmospheric mixing captured more effectively by
701 satellite observations at greater distances from roads. Using a larger buffer distance from roads
702 (300 meters instead of 50 meters) improves the alignment between TROPOMI and monitor data,
703 especially for highway monitor locations (JSD decreases by ~82%). The overall trend reflects the

704 well-established gradient of declining NO₂ levels with increasing distance from traffic sources,
705 and TROPOMI's ability to capture this trend, even if the specific values differ from AQS
706 monitors in the near-road environment. Our findings indicate that TROPOMI tends to slightly
707 underestimate surface NO₂ concentrations in areas with high traffic, such as interstates and
708 highways, due to its spatial resolution and full-column measurements, which smooth out
709 localized, ground-level pollution peaks captured by ground monitors. This is most evident in
710 interstate monitors, where the JSD reveals the greatest divergence between satellite and monitor
711 data (JSD = 0.158). These results are consistent with prior studies (Dressel et al., 2022; Kim et
712 al., 2024; Ialongo et al., 2020), which also found that satellite instruments are less effective at
713 capturing high NO₂ events near localized sources like traffic. The distributional alignment
714 improves in non-roadway monitors (JSD = 0.009), where NO₂ levels are lower, and there are
715 usually fewer localized sources of pollution. The lower pollution levels in these areas allow
716 TROPOMI to more accurately reflect the conditions captured by ground-based monitors, leading
717 to lower JSD values, and therefore better alignment. This trend suggests that TROPOMI may be
718 particularly useful for monitoring air quality in rural or less polluted regions where ground
719 monitors are sparse or absent.

720 Seasonality plays a critical role in the similarity of satellite and monitor data. Winter consistently
721 shows the best alignment (JSD = 0.010), with the TROPOMI distribution capturing nearly the
722 full gradient of NO₂ seen within the ground-based monitor distribution. This likely reflects the
723 longer atmospheric lifetime of NO₂ in winter, which allows for better vertical mixing and less
724 spatial variability (Harkey et al., 2015; Boersma et al., 2009; Shah et al., 2020). In contrast,
725 summer shows the worst alignment (JSD = 0.035), which is likely due to the shorter lifetime of
726 NO₂ and increased photochemical activity during warmer months, causing greater discrepancies
727 between localized surface measurements and the satellite column. Similar conclusions were
728 reached by previous studies (Shah et al., 2020; Karagkiozidis et al., 2023), indicating that
729 seasonality is a crucial factor in assessing satellite performance for regulatory purposes. These
730 seasonal differences underscore the need for considering temporal factors when evaluating the
731 use of satellite data for monitor siting and NO₂ regulation.

732 The integration of TEMPO data into this study highlights its potential to advance our
733 understanding of NO₂ distributions, especially when compared to TROPOMI. TEMPO's ability

734 to provide hourly measurements at a finer spatial resolution offers significant advantages in
735 capturing diurnal NO₂ patterns and detecting localized pollution events. Our findings from
736 December 2023 and July 2024 at the TROPOMI overpass time (~13:30 LST) demonstrate that
737 TEMPO better captures the wide range of surface NO₂ measurements than TROPOMI,
738 especially at higher NO₂ levels. TEMPO's JSDs are almost always lower than TROPOMI's, with
739 JSDs ranging from 0.005 to 0.151 and TROPOMI's JSDs ranging from 0.012 to 0.265. This
740 improvement in alignment with ground monitors could be attributed to TEMPO's better spatial
741 and temporal resolution.

742 We also find that TEMPO is best at capturing ground-level NO₂ amounts around midday (~10am
743 to ~2pm LT). This could be due to the lower traffic levels and therefore lower pollution levels
744 during this time period, as well as a lower solar zenith angle, allowing TEMPO to have more
745 accurate measurements. However, challenges remain in completely capturing high NO₂ levels
746 during peak traffic times and accurately capturing NO₂ during high solar zenith angles in the
747 morning and evening across monitor classifications. These results underscore the influence of
748 spatial resolution, time of day, and measurement frequency on the ability of satellite instruments
749 to align with ground-based NO₂ measurements. Future research should build upon these insights
750 by incorporating longer time periods and multiple years of data as more TEMPO data becomes
751 available to study long-term TEMPO distributions. The enhanced temporal and spatial resolution
752 of TEMPO, alongside its comparison to other instruments like TROPOMI, provides valuable
753 context for understanding the dynamics of NO₂ pollution, especially how it varies throughout the
754 day, to improve strategies for air quality monitoring and public health protection. Spatially
755 contiguous satellite products and our analysis of air quality variability offer the potential to
756 support air quality managers and public health analysis.

757 This study offers insights for optimizing nitrogen dioxide monitor siting, enhancing regulatory
758 planning, and supporting public health interventions. By demonstrating the strengths and
759 limitations of satellite-derived NO₂ data, we highlight its potential to complement ground-based
760 monitoring networks.

761

762 **Code and Data Availability**

763 All data used in this study are open to the public. Hourly NO₂ data from AQS were obtained
764 from https://aqs.epa.gov/aqsweb/airdata/download_files.html. Copernicus Sentinel 5P Level 2
765 TROPOMI NO₂ data were processed by the ESA, Koninklijk Nederlands Meteorologisch
766 Instituut (KNMI; <https://doi.org/10.5270/S5P-s4ljg54>), downloaded from the NASA Goddard
767 Earth Sciences Data and Information Center (GES DISC) in January 2021, and gridded using
768 WHIPS (<https://sage.nelson.wisc.edu/data-and-models/wisconsin-horizontal-interpolation-program-for-satellites-whips/>). TEMPO Level 3 NO₂ data were downloaded from NASA's
769 EarthData Search ([https://search.earthdata.nasa.gov/search/granules?p=C2930763263-LARC_CLOUD&pg\[0\]\[v\]=f&tl=1732652660.361!3!!](https://search.earthdata.nasa.gov/search/granules?p=C2930763263-LARC_CLOUD&pg[0][v]=f&tl=1732652660.361!3!!)). [The 2021 Primary and Secondary Roads](https://www.census.gov/cgi-bin/geo/shapefiles/index.php?year=2021&layergroup=Roads)
770 [Tiger/Line state-level shapefiles were downloaded from the U.S. Census Bureau](https://www.census.gov/cgi-bin/geo/shapefiles/index.php?year=2021&layergroup=Roads)
771 (<https://www.census.gov/cgi-bin/geo/shapefiles/index.php?year=2021&layergroup=Roads>).
772 Since all of our data is publicly available and the methods describe our calculations in detail, we
773 did not make our code publicly available. The Jensen Shannon Divergence was calculated using
774 the *scipy.spatial.distance.jensenshannon* python package.

775

776 **Author Contribution**

777 SA and TH conceptualized and designed methodology. MH helped with data curation. SA
778 performed data analysis and visualization and prepared the original draft of the manuscript. All
779 authors contributed to reviewing and editing the manuscript.

780

781 **Competing Interests**

782 The authors declare that they have no conflict of interest.

783

784 **Acknowledgements**

785 This paper was funded by NASA Grant 80NSSC21K0427 through the Health and Air Quality
786 Applied Sciences Team (HAQAST). We also thank the EPA for providing the Air Quality System
787 data, the Earth Sciences Data and Information Center (GES DISC) for TROPOMI L2 data, the
788 Wisconsin Horizontal Interpolation Program for Satellites (WHIPS) for helping to process and
789 grid TROPOMI data, and NASA Langley Atmospheric Science Data Center Distributed Active
790

792 Archive Center for providing access to the TEMPO data. The authors acknowledge OpenAI 4o
793 for help with data analysis debugging.

794

795

796 **References**

797 Achakulwisut, P., Brauer, M., Hystad, P., and Anenberg, S. C.: Global, national, and urban
798 burdens of paediatric asthma incidence attributable to ambient NO₂ pollution: estimates from
799 global datasets, *The Lancet Planetary Health*, 3, e166–e178, [https://doi.org/10.1016/S2542-
800 5196\(19\)30046-4](https://doi.org/10.1016/S2542-5196(19)30046-4), 2019.

801 Aerts, S., Haesbroeck, G., and Ruwet, C.: Multivariate coefficients of variation: Comparison and
802 influence functions, *Journal of Multivariate Analysis*, 142, 183–198,
803 <https://doi.org/10.1016/j.jmva.2015.08.006>, 2015.

804 Ahmed, Z., Zeeshan, S., Persaud, N., Degroat, W., Abdelhalim, H., and Liang, B. T.:
805 Investigating genes associated with cardiovascular disease among heart failure patients for
806 translational research and precision medicine, *Clinical and Translational Dis*, 3, e206,
807 <https://doi.org/10.1002/ctd2.206>, 2023.

808 Anenberg, S. C., Mohegh, A., Goldberg, D. L., Kerr, G. H., Brauer, M., Burkart, K., Hystad, P.,
809 Larkin, A., Wozniak, S., and Lamsal, L.: Long-term trends in urban NO₂ concentrations and
810 associated paediatric asthma incidence: estimates from global datasets, *The Lancet Planetary
811 Health*, 6, e49–e58, [https://doi.org/10.1016/S2542-5196\(21\)00255-2](https://doi.org/10.1016/S2542-5196(21)00255-2), 2022.

812 Bai, L., Chen, H., Hatzopoulou, M., Jerrett, M., Kwong, J. C., Burnett, R. T., Van Donkelaar, A.,
813 Copes, R., Martin, R. V., Van Ryswyk, K., Lu, H., Kopp, A., and Weichenthal, S.: Exposure to
814 Ambient Ultrafine Particles and Nitrogen Dioxide and Incident Hypertension and Diabetes:,
815 *Epidemiology*, 29, 323–332, <https://doi.org/10.1097/EDE.0000000000000798>, 2018.

816 Bechle, M. J., Millet, D. B., and Marshall, J. D.: Remote sensing of exposure to NO₂: Satellite
817 versus ground-based measurement in a large urban area, *Atmospheric Environment*, 69, 345–
818 353, <https://doi.org/10.1016/j.atmosenv.2012.11.046>, 2013.

819 Behera, S. N. and Sharma, M.: Transformation of atmospheric ammonia and acid gases into
820 components of PM_{2.5}: an environmental chamber study, Environ Sci Pollut Res, 19, 1187–1197,
821 <https://doi.org/10.1007/s11356-011-0635-9>, 2012.

822 Boersma, K. F., Jacob, D. J., Trainic, M., Rudich, Y., DeSmedt, I., Dirksen, R., and Eskes, H. J.:
823 Validation of urban NO₂ concentrations and their diurnal and seasonal
824 variations observed from the SCIAMACHY and OMI sensors using in situ surface
825 measurements in Israeli cities, Atmos. Chem. Phys., 9, 3867–3879, <https://doi.org/10.5194/acp-9-3867-2009>, 2009.

826 Boersma, K. F., Eskes, H. J., Richter, A., De Smedt, I., Lorente, A., Beirle, S., Van Geffen, J. H.
827 G. M., Zara, M., Peters, E., Van Roozendael, M., Wagner, T., Maasakkers, J. D., Van Der A, R. J.,
828 Nightingale, J., De Rudder, A., Irie, H., Pinardi, G., Lambert, J.-C., and Compernolle, S. C.:
829 Improving algorithms and uncertainty estimates for satellite NO₂ retrievals: results from the quality
830 assurance for the essential climate variables (QA4ECV) project, Atmos. Meas. Tech., 11, 6651–6678, <https://doi.org/10.5194/amt-11-6651-2018>, 2018.

831 Camilleri, S. F., Kerr, G. H., Anenberg, S. C., and Horton, D. E.: All-Cause NO₂ -Attributable
832 Mortality Burden and Associated Racial and Ethnic Disparities in the United States, Environ.
833 Sci. Technol. Lett., 10, 1159–1164, <https://doi.org/10.1021/acs.estlett.3c00500>, 2023.

834 Wisconsin Horizontal Interpolation Program for Satellites (WHIPS):
835 <https://sage.nelson.wisc.edu/data-and-models/wisconsin-horizontal-interpolation-program-for-satellites-whips/>, last access: 6 December 2024.

836 Chance, K., Liu, X., Miller, C. C., González Abad, G., Huang, G., Nowlan, C., Souri, A.,
837 Suleiman, R., Sun, K., Wang, H., Zhu, L., Zoogman, P., Al-Saadi, J., Antuña-Marrero, J.-C., Carr,
838 J., Chatfield, R., Chin, M., Cohen, R., Edwards, D., Fishman, J., Flittner, D., Geddes, J., Grutter,
839 M., Herman, J. R., Jacob, D. J., Janz, S., Joiner, J., Kim, J., Krotkov, N. A., Lefer, B., Martin, R.
840 V., Mayol-Bracero, O. L., Naeger, A., Newchurch, M., Pfister, G. G., Pickering, K., Pierce, R. B.,
841 Rivera Cárdenas, C., Saiz-Lopez, A., Simpson, W., Spinei, E., Spurr, R. J. D., Szykman, J. J.,
842 Torres, O., and Wang, J.: TEMPO Green Paper: Chemistry, physics, and meteorology
843 experiments with the Tropospheric Emissions: monitoring of pollution instrument, in: Sensors,
844 845

847 Systems, and Next-Generation Satellites XXIII, Sensors, Systems, and Next-Generation
848 Satellites XXIII, Strasbourg, France, 10, <https://doi.org/10.1117/12.2534883>, 2019.

849 Chowdhury, S., Haines, A., Klingmüller, K., Kumar, V., Pozzer, A., Venkataraman, C., Witt, C.,
850 and Lelieveld, J.: Global and national assessment of the incidence of asthma in children and
851 adolescents from major sources of ambient NO₂, Environ. Res. Lett., 16, 035020,
852 <https://doi.org/10.1088/1748-9326/abe909>, 2021.

853 Clim, A., Zota, R. D., and Tinică, G.: The Kullback-Leibler Divergence Used in Machine
854 Learning Algorithms for Health Care Applications and Hypertension Prediction: A Literature
855 Review, Procedia Computer Science, 141, 448–453, <https://doi.org/10.1016/j.procs.2018.10.144>,
856 2018.

857 Cooper, M. J., Martin, R. V., McLinden, C. A., and Brook, J. R.: Inferring ground-level nitrogen
858 dioxide concentrations at fine spatial resolution applied to the TROPOMI satellite instrument,
859 Environ. Res. Lett., 15, 104013, <https://doi.org/10.1088/1748-9326/aba3a5>, 2020.

860 Dang, R., Jacob, D. J., Shah, V., Eastham, S. D., Fritz, T. M., Mickley, L. J., Liu, T., Wang, Y.,
861 and Wang, J.: Background nitrogen dioxide (NO₂) over the United States and its implications for
862 satellite observations and trends: effects of nitrate photolysis, aircraft, and open fires, Atmos.
863 Chem. Phys., 23, 6271–6284, <https://doi.org/10.5194/acp-23-6271-2023>, 2023.

864 Dressel, I. M., Demetillo, M. A. G., Judd, L. M., Janz, S. J., Fields, K. P., Sun, K., Fiore, A. M.,
865 McDonald, B. C., and Pusede, S. E.: Daily Satellite Observations of Nitrogen Dioxide Air
866 Pollution Inequality in New York City, New York and Newark, New Jersey: Evaluation and
867 Application, Environ. Sci. Technol., 56, 15298–15311, <https://doi.org/10.1021/acs.est.2c02828>,
868 2022.

869 Duncan, B. N., Yoshida, Y., De Foy, B., Lamsal, L. N., Streets, D. G., Lu, Z., Pickering, K. E.,
870 and Krotkov, N. A.: The observed response of Ozone Monitoring Instrument (OMI) NO₂
871 columns to NO_x emission controls on power plants in the United States: 2005–2011,
872 Atmospheric Environment, 81, 102–111, <https://doi.org/10.1016/j.atmosenv.2013.08.068>, 2013.

873 Duncan, B. N., Prados, A. I., Lamsal, L. N., Liu, Y., Streets, D. G., Gupta, P., Hilsenrath, E.,
874 Kahn, R. A., Nielsen, J. E., Beyersdorf, A. J., Burton, S. P., Fiore, A. M., Fishman, J., Henze, D.

875 K., Hostetler, C. A., Krotkov, N. A., Lee, P., Lin, M., Pawson, S., Pfister, G., Pickering, K. E.,
876 Pierce, R. B., Yoshida, Y., and Ziemba, L. D.: Satellite data of atmospheric pollution for U.S. air
877 quality applications: Examples of applications, summary of data end-user resources, answers to
878 FAQs, and common mistakes to avoid, *Atmospheric Environment*, 94, 647–662,
879 <https://doi.org/10.1016/j.atmosenv.2014.05.061>, 2014.

880 Dunlea, E. J., Herndon, S. C., Nelson, D. D., Volkamer, R. M., San Martini, F., Sheehy, P. M.,
881 Zahniser, M. S., Shorter, J. H., Wormhoudt, J. C., Lamb, B. K., Allwine, E. J., Gaffney, J. S.,
882 Marley, N. A., Grutter, M., Marquez, C., Blanco, S., Cardenas, B., Retama, A., Ramos Villegas,
883 C. R., Kolb, C. E., Molina, L. T., and Molina, M. J.: Evaluation of nitrogen dioxide
884 chemiluminescence monitors in a polluted urban environment, *Atmos. Chem. Phys.*, 7, 2691–
885 2704, <https://doi.org/10.5194/acp-7-2691-2007>, 2007.

886 AirData Pre-Generated Hourly File Downloads:
887 https://aqs.epa.gov/aqsweb/airdata/download_files.html#Raw, last access: 21 February 2025.

888 European Space Agency: TROPOMI Level 2 Nitrogen Dioxide, <https://doi.org/10.5270/S5P-9bnp8q8>, 2021.

889 Fontijn, Arthur., Sabadell, A. J., and Ronco, R. J.: Homogeneous chemiluminescent measurement
890 of nitric oxide with ozone. Implications for continuous selective monitoring of gaseous air
891 pollutants, *Anal. Chem.*, 42, 575–579, <https://doi.org/10.1021/ac60288a034>, 1970.

892 Frost, G. J., McKeen, S. A., Trainer, M., Ryerson, T. B., Neuman, J. A., Roberts, J. M., Swanson,
893 A., Holloway, J. S., Sueper, D. T., Fortin, T., Parrish, D. D., Fehsenfeld, F. C., Flocke, F.,
894 Peckham, S. E., Grell, G. A., Kowal, D., Cartwright, J., Auerbach, N., and Habermann, T.:
895 Effects of changing power plant NO_x emissions on ozone in the eastern United States: Proof of
896 concept, *J. Geophys. Res.*, 111, 2005JD006354, <https://doi.org/10.1029/2005JD006354>, 2006.

897 Gantt, B., Owen, R. C., and Watkins, N.: Characterizing Nitrogen Oxides and Fine Particulate
898 Matter near Major Highways in the United States Using the National Near-Road Monitoring
899 Network, *Environ. Sci. Technol.*, 55, 2831–2838, <https://doi.org/10.1021/acs.est.0c05851>, 2021.

900 Ge, B., Sun, Y., Liu, Y., Dong, H., Ji, D., Jiang, Q., Li, J., and Wang, Z.: Nitrogen dioxide
901 measurement by cavity attenuated phase shift spectroscopy (CAPS) and implications in ozone

903 production efficiency and nitrate formation in Beijing, China, JGR Atmospheres, 118, 9499–
904 9509, <https://doi.org/10.1002/jgrd.50757>, 2013.

905 Goldberg, D. L., Anenberg, S. C., Kerr, G. H., Mohegh, A., Lu, Z., and Streets, D. G.:
906 TROPOMI NO₂ in the United States: A Detailed Look at the Annual Averages, Weekly Cycles,
907 Effects of Temperature, and Correlation With Surface NO₂ Concentrations, Earth's Future, 9,
908 e2020EF001665, <https://doi.org/10.1029/2020EF001665>, 2021.

909 Goldberg, D. L., Tao, M., Kerr, G. H., Ma, S., Tong, D. Q., Fiore, A. M., Dickens, A. F.,
910 Adelman, Z. E., and Anenberg, S. C.: Evaluating the spatial patterns of U.S. urban NO_x
911 emissions using TROPOMI NO₂, Remote Sensing of Environment, 300, 113917,
912 <https://doi.org/10.1016/j.rse.2023.113917>, 2024.

913 Griffin, D., Zhao, X., McLinden, C. A., Boersma, F., Bourassa, A., Dammers, E., Degenstein, D.,
914 Eskes, H., Fehr, L., Fioletov, V., Hayden, K., Kharol, S. K., Li, S., Makar, P., Martin, R. V.,
915 Mihele, C., Mittermeier, R. L., Krotkov, N., Sneep, M., Lamsal, L. N., Linden, M. T., Geffen, J.
916 V., Veefkind, P., and Wolde, M.: High-Resolution Mapping of Nitrogen Dioxide With
917 TROPOMI: First Results and Validation Over the Canadian Oil Sands, Geophysical Research
918 Letters, 46, 1049–1060, <https://doi.org/10.1029/2018GL081095>, 2019.

919 Grulke, N. E. and Heath, R. L.: Ozone effects on plants in natural ecosystems, Plant Biol J, 22,
920 12–37, <https://doi.org/10.1111/plb.12971>, 2020.

921 Hales, S., Atkinson, J., Metcalfe, J., Kuschel, G., and Woodward, A.: Long term exposure to air
922 pollution, mortality and morbidity in New Zealand: Cohort study, Science of The Total
923 Environment, 801, 149660, <https://doi.org/10.1016/j.scitotenv.2021.149660>, 2021.

924 Harkey, M. and Holloway, T.: Simulated Surface-Column NO₂ Connections for Satellite
925 Applications, JGR Atmospheres, 129, e2024JD041912, <https://doi.org/10.1029/2024JD041912>,
926 2024.

927 Harkey, M., Holloway, T., Oberman, J., and Scotty, E.: An evaluation of CMAQ NO₂ using
928 observed chemistry-meteorology correlations, JGR Atmospheres, 120,
929 <https://doi.org/10.1002/2015JD023316>, 2015.

930 Harkey, M., Holloway, T., Kim, E. J., Baker, K. R., and Henderson, B.: Satellite Formaldehyde to
931 Support Model Evaluation, *JGR Atmospheres*, 126, e2020JD032881,
932 <https://doi.org/10.1029/2020JD032881>, 2021.

933 Holloway, T., Miller, D., Anenberg, S., Diao, M., Duncan, B., Fiore, A. M., Henze, D. K., Hess,
934 J., Kinney, P. L., Liu, Y., Neu, J. L., O'Neill, S. M., Odman, M. T., Pierce, R. B., Russell, A. G.,
935 Tong, D., West, J. J., and Zondlo, M. A.: Satellite Monitoring for Air Quality and Health, *Annu.
936 Rev. Biomed. Data Sci.*, 4, 417–447, <https://doi.org/10.1146/annurev-biodatasci-110920-093120>,
937 2021.

938 Huangfu, P. and Atkinson, R.: Long-term exposure to NO₂ and O₃ and all-cause and respiratory
939 mortality: A systematic review and meta-analysis, *Environment International*, 144, 105998,
940 <https://doi.org/10.1016/j.envint.2020.105998>, 2020.

941 Huber, D. E., Steiner, A. L., and Kort, E. A.: Daily Cropland Soil NO_x Emissions Identified by
942 TROPOMI and SMAP, *Geophysical Research Letters*, 47, e2020GL089949,
943 <https://doi.org/10.1029/2020GL089949>, 2020.

944 Ialongo, I., Virta, H., Eskes, H., Hovila, J., and Douros, J.: Comparison of TROPOMI/Sentinel-5
945 Precursor NO₂ observations with ground-based measurements in
946 Helsinki, *Atmos. Meas. Tech.*, 13, 205–218, <https://doi.org/10.5194/amt-13-205-2020>, 2020.

947 Jia, M., Wang, Z., Wang, C., Mao, D., and Zhang, Y.: A New Vegetation Index to Detect
948 Periodically Submerged Mangrove Forest Using Single-Tide Sentinel-2 Imagery, *Remote
949 Sensing*, 11, 2043, <https://doi.org/10.3390/rs11172043>, 2019.

950 Jones, D. C., Danaher, P., Kim, Y., Beechem, J. M., Gottardo, R., and Newell, E. W.: An
951 information theoretic approach to detecting spatially varying genes, *Cell Reports Methods*, 3,
952 100507, <https://doi.org/10.1016/j.crmeth.2023.100507>, 2023.

953 Kang, D. and Pickering, K.: Lightning NO_x Emissions and the Implications for Surface Air
954 Quality over the Contiguous United States, *EM (Pittsburgh Pa)*, 11, 1–6, 2018.

955 Karagkiozidis, D., Koukouli, M.-E., Bais, A., Balis, D., and Tzoumaka, P.: Assessment of the
956 NO₂ Spatio-Temporal Variability over Thessaloniki, Greece, Using MAX-DOAS Measurements

957 and Comparison with S5P/TROPOMI Observations, Applied Sciences, 13, 2641,
958 <https://doi.org/10.3390/app13042641>, 2023.

959 Karner, A. A., Eisinger, D. S., and Niemeier, D. A.: Near-Roadway Air Quality: Synthesizing the
960 Findings from Real-World Data, Environ. Sci. Technol., 44, 5334–5344,
961 <https://doi.org/10.1021/es100008x>, 2010.

962 Kebabian, P. L., Herndon, S. C., and Freedman, A.: Detection of Nitrogen Dioxide by Cavity
963 Attenuated Phase Shift Spectroscopy, Anal. Chem., 77, 724–728,
964 <https://doi.org/10.1021/ac048715y>, 2005.

965 Kerr, G. H., Goldberg, D. L., Harris, M. H., Henderson, B. H., Hystad, P., Roy, A., and
966 Anenberg, S. C.: Ethnoracial Disparities in Nitrogen Dioxide Pollution in the United States:
967 Comparing Data Sets from Satellites, Models, and Monitors, Environ. Sci. Technol., 57, 19532–
968 19544, <https://doi.org/10.1021/acs.est.3c03999>, 2023.

969 Kibirige, G. W., Huang, C. C., Liu, C. L., and Chen, M. C.: Influence of land-sea breeze on
970 PM_{2.5} prediction in central and southern Taiwan using composite neural network, Sci
971 Rep., 13, 3827, <https://doi.org/10.1038/s41598-023-29845-w>, 2023.

972 Kim, E. J., Holloway, T., Kokandakar, A., Harkey, M., Elkins, S., Goldberg, D. L., and Heck, C.:
973 A Comparison of Regression Methods for Inferring Near-Surface NO₂ With Satellite Data, JGR
974 Atmospheres, 129, e2024JD040906, <https://doi.org/10.1029/2024JD040906>, 2024.

975 Kim, H. C., Kim, S., Lee, S.-H., Kim, B.-U., and Lee, P.: Fine-Scale Columnar and Surface NO_x
976 Concentrations over South Korea: Comparison of Surface Monitors, TROPOMI, CMAQ and
977 CAPSS Inventory, Atmosphere, 11, 101, <https://doi.org/10.3390/atmos11010101>, 2020.

978 Kim, M., Brunner, D., and Kuhlmann, G.: Importance of satellite observations for high-
979 resolution mapping of near-surface NO₂ by machine learning, Remote Sensing of Environment,
980 264, 112573, <https://doi.org/10.1016/j.rse.2021.112573>, 2021.

981 Kimbrough, S., Chris Owen, R., Snyder, M., and Richmond-Bryant, J.: NO to NO₂ conversion
982 rate analysis and implications for dispersion model chemistry methods using Las Vegas, Nevada
983 near-road field measurements, Atmospheric Environment, 165, 23–34,
984 <https://doi.org/10.1016/j.atmosenv.2017.06.027>, 2017.

985 Knox, J. B. and Lange, R.: Surface Air Pollutant Concentration Frequency Distributions:
986 Implications for Urban Modeling, *Journal of the Air Pollution Control Association*, 24, 48–53,
987 <https://doi.org/10.1080/00022470.1974.10469893>, 1974.

988 Lamsal, L. N., Krotkov, N. A., Celarier, E. A., Swartz, W. H., Pickering, K. E., Bucsela, E. J.,
989 Gleason, J. F., Martin, R. V., Philip, S., Irie, H., Cede, A., Herman, J., Weinheimer, A., Szykman,
990 J. J., and Knepp, T. N.: Evaluation of OMI operational standard NO₂ column retrievals using in situ and surface-based NO₂ observations, *Atmos. Chem. Phys.*, 14, 11587–11609, <https://doi.org/10.5194/acp-14-11587-2014>, 2014.

993 Lamsal, L. N., Duncan, B. N., Yoshida, Y., Krotkov, N. A., Pickering, K. E., Streets, D. G., and
994 Lu, Z.: U.S. NO₂ trends (2005–2013): EPA Air Quality System (AQS) data versus improved
995 observations from the Ozone Monitoring Instrument (OMI), *Atmospheric Environment*, 110,
996 130–143, <https://doi.org/10.1016/j.atmosenv.2015.03.055>, 2015.

997 Lange, K., Richter, A., and Burrows, J. P.: Variability of nitrogen oxide emission fluxes and
998 lifetimes estimated from Sentinel-5P TROPOMI observations, *Atmos. Chem. Phys.*, 22, 2745–
999 2767, <https://doi.org/10.5194/acp-22-2745-2022>, 2022.

1000 Lee, H. J. and Koutrakis, P.: Daily Ambient NO₂ Concentration Predictions Using Satellite
1001 Ozone Monitoring Instrument NO₂ Data and Land Use Regression, *Environ. Sci. Technol.*,
1002 140204134232009, <https://doi.org/10.1021/es404845f>, 2014.

1003 Lee, H. J., Liu, Y., and Chatfield, R. B.: Neighborhood-scale ambient NO₂ concentrations using
1004 TROPOMI NO₂ data: Applications for spatially comprehensive exposure assessment, *Science of
1005 The Total Environment*, 857, 159342, <https://doi.org/10.1016/j.scitotenv.2022.159342>, 2023.

1006 Lee, M., Heikes, B. G., Jacob, D. J., Sachse, G., and Anderson, B.: Hydrogen peroxide, organic
1007 hydroperoxide, and formaldehyde as primary pollutants from biomass burning, *J. Geophys. Res.*,
1008 102, 1301–1309, <https://doi.org/10.1029/96JD01709>, 1997.

1009 Levinson, R. and Akbari, H.: Potential benefits of cool roofs on commercial buildings:
1010 conserving energy, saving money, and reducing emission of greenhouse gases and air pollutants,
1011 *Energy Efficiency*, 3, 53–109, <https://doi.org/10.1007/s12053-008-9038-2>, 2010.

1012 Li, J., Wang, Y., Zhang, R., Smeltzer, C., Weinheimer, A., Herman, J., Boersma, K. F., Celarier,
1013 E. A., Long, R. W., Szykman, J. J., Delgado, R., Thompson, A. M., Knapp, T. N., Lamsal, L. N.,
1014 Janz, S. J., Kowalewski, M. G., Liu, X., and Nowlan, C. R.: Comprehensive evaluations of
1015 diurnal NO₂ measurements during DISCOVER-AQ 2011: effects of
1016 resolution-dependent representation of NO₂; Atmos. Chem. Phys., 21, 11133–11160, <https://doi.org/10.5194/acp-21-11133-2021>,
1017 2021.

1019 Liu, X., Yi, G., Zhou, X., Zhang, T., Lan, Y., Yu, D., Wen, B., and Hu, J.: Atmospheric NO₂
1020 Distribution Characteristics and Influencing Factors in Yangtze River Economic Belt: Analysis of
1021 the NO₂ Product of TROPOMI/Sentinel-5P, Atmosphere, 12, 1142,
1022 <https://doi.org/10.3390/atmos12091142>, 2021.

1023 Melville, P., Yang, S.M., Saar-Tsechansky, M., Mooney, R.J.: Active Learning for Probability
1024 Estimation using Jensen-Shannon Divergence, in: Proceedings of the 16th European Conference
1025 on Machine Learning, 268–279, 2005.

1026 Menéndez, M. L., Pardo, J. A., Pardo, L., and Pardo, M. C.: The Jensen-Shannon divergence,
1027 Journal of the Franklin Institute, 334, 307–318, [https://doi.org/10.1016/S0016-0032\(96\)00063-4](https://doi.org/10.1016/S0016-0032(96)00063-4),
1028 1997.

1029 Meng, X., Liu, C., Chen, R., Sera, F., Vicedo-Cabrera, A. M., Milojevic, A., Guo, Y., Tong, S.,
1030 Coelho, M. D. S. Z. S., Saldiva, P. H. N., Lavigne, E., Correa, P. M., Ortega, N. V., Osorio, S.,
1031 Garcia, Kyselý, J., Urban, A., Orru, H., Maasikmets, M., Jaakkola, J. J. K., Rytí, N., Huber, V.,
1032 Schneider, A., Katsouyanni, K., Analitis, A., Hashizume, M., Honda, Y., Ng, C. F. S., Nunes, B.,
1033 Teixeira, J. P., Holobaca, I. H., Fratianni, S., Kim, H., Tobias, A., Íñiguez, C., Forsberg, B.,
1034 Åström, C., Ragettli, M. S., Guo, Y.-L. L., Pan, S.-C., Li, S., Bell, M. L., Zanobetti, A., Schwartz,
1035 J., Wu, T., Gasparrini, A., and Kan, H.: Short term associations of ambient nitrogen dioxide with
1036 daily total, cardiovascular, and respiratory mortality: multilocation analysis in 398 cities, BMJ,
1037 n534, <https://doi.org/10.1136/bmj.n534>, 2021.

1038 Mills, I. C., Atkinson, R. W., Kang, S., Walton, H., and Anderson, H. R.: Quantitative systematic
1039 review of the associations between short-term exposure to nitrogen dioxide and mortality and

1040 hospital admissions, BMJ Open, 5, e006946, <https://doi.org/10.1136/bmjopen-2014-006946>,
1041 2015.

1042 Mölter, A., Agius, R., De Vocht, F., Lindley, S., Gerrard, W., Custovic, A., and Simpson, A.:
1043 Effects of long-term exposure to PM₁₀ and NO₂ on asthma and wheeze in a prospective birth
1044 cohort, J Epidemiol Community Health, 68, 21–28, <https://doi.org/10.1136/jech-2013-202681>,
1045 2014.

1046 Mondal, A., Sharma, S. K., Mandal, T. K., Girach, I., and Ojha, N.: Frequency distribution of
1047 pollutant concentrations over Indian megacities impacted by the COVID-19 lockdown, Environ
1048 Sci Pollut Res, 29, 85676–85687, <https://doi.org/10.1007/s11356-021-16874-z>, 2022.

1049 Naeger, A. R., Newchurch, M. J., Moore, T., Chance, K., Liu, X., Alexander, S., Murphy, K., and
1050 Wang, B.: Revolutionary Air-Pollution Applications from Future Tropospheric Emissions:
1051 Monitoring of Pollution (TEMPO) Observations, Bulletin of the American Meteorological
1052 Society, 102, E1735–E1741, <https://doi.org/10.1175/BAMS-D-21-0050.1>, 2021.

1053 Tropospheric Emissions: Monitoring of Pollution (EVI-1) | NASA's Earth Observing System:
1054 <https://eospso.nasa.gov/missions/tropospheric-emissions-monitoring-pollution-evi-1>, last access:
1055 26 November 2024.

1056 NASA Langley Research Center: TEMPO Level 2/3 trace gas and cloud data user guide, 2024.

1057 Novotny, E. V., Bechle, M. J., Millet, D. B., and Marshall, J. D.: National Satellite-Based Land-
1058 Use Regression: NO₂ in the United States, Environ. Sci. Technol., 45, 4407–4414,
1059 <https://doi.org/10.1021/es103578x>, 2011.

1060 Orellano, P., Reynoso, J., Quaranta, N., Bardach, A., and Ciapponi, A.: Short-term exposure to
1061 particulate matter (PM10 and PM2.5), nitrogen dioxide (NO₂), and ozone (O₃) and all-cause and
1062 cause-specific mortality: Systematic review and meta-analysis, Environment International, 142,
1063 105876, <https://doi.org/10.1016/j.envint.2020.105876>, 2020.

1064 Penn, E. and Holloway, T.: Evaluating current satellite capability to observe diurnal change in
1065 nitrogen oxides in preparation for geostationary satellite missions, Environ. Res. Lett., 15,
1066 034038, <https://doi.org/10.1088/1748-9326/ab6b36>, 2020.

1067 Pollack, R.: Studies of Pollutant Concentration Frequency Distributions, 1975.

1068 Qin, M., Yu, H., Hu, Y., Russell, A. G., Odman, M. T., Doty, K., Pour-Biazar, A., McNider, R. T.,
1069 and Knipping, E.: Improving ozone simulations in the Great Lakes Region: The role of
1070 emissions, chemistry, and dry deposition, *Atmospheric Environment*, 202, 167–179,
1071 <https://doi.org/10.1016/j.atmosenv.2019.01.025>, 2019.

1072 Richmond-Bryant, J., Chris Owen, R., Graham, S., Snyder, M., McDow, S., Oakes, M., and
1073 Kimbrough, S.: Estimation of on-road NO₂ concentrations, NO₂/NO_X ratios, and related
1074 roadway gradients from near-road monitoring data, *Air Qual Atmos Health*, 10, 611–625,
1075 <https://doi.org/10.1007/s11869-016-0455-7>, 2017.

1076 Richter, A., Burrows, J. P., Nüß, H., Granier, C., and Niemeier, U.: Increase in tropospheric
1077 nitrogen dioxide over China observed from space, *Nature*, 437, 129–132,
1078 <https://doi.org/10.1038/nature04092>, 2005.

1079 Sangkham, S., Phairuang, W., Sherchan, S. P., Pansakun, N., Munkong, N., Sarndhong, K.,
1080 Islam, Md. A., and Sakunkoo, P.: An update on adverse health effects from exposure to PM_{2.5},
1081 *Environmental Advances*, 18, 100603, <https://doi.org/10.1016/j.envadv.2024.100603>, 2024.

1082 Saurette, D. D., Heck, R. J., Gillespie, A. W., Berg, A. A., and Biswas, A.: Divergence metrics for
1083 determining optimal training sample size in digital soil mapping, *Geoderma*, 436, 116553,
1084 <https://doi.org/10.1016/j.geoderma.2023.116553>, 2023.

1085 Shah, V., Jacob, D. J., Li, K., Silvern, R. F., Zhai, S., Liu, M., Lin, J., and Zhang, Q.: Effect of
1086 changing NO₂ lifetime on the seasonality and long-
1087 term trends of satellite-observed tropospheric NO₂ columns over China,
1088 *Atmos. Chem. Phys.*, 20, 1483–1495, <https://doi.org/10.5194/acp-20-1483-2020>, 2020.

1089 Sharma, S., Chandra, M., and Kota, S. H.: Health Effects Associated with PM_{2.5}: a Systematic
1090 Review, *Curr Pollution Rep*, 6, 345–367, <https://doi.org/10.1007/s40726-020-00155-3>, 2020.

1091 Shetty, S., Schneider, P., Stebel, K., David Hamer, P., Kylling, A., and Karen Berntsen, T.:
1092 Estimating surface NO₂ concentrations over Europe using Sentinel-5P TROPOMI observations
1093 and Machine Learning, *Remote Sensing of Environment*, 312, 114321,
1094 <https://doi.org/10.1016/j.rse.2024.114321>, 2024.

1095 Sillman, S.: The relation between ozone, NOx and hydrocarbons in urban and polluted rural
1096 environments, *Atmospheric Environment*, 33, 1821–1845, [https://doi.org/10.1016/S1352-
1097 2310\(98\)00345-8](https://doi.org/10.1016/S1352-2310(98)00345-8), 1999.

1098 Steinbacher, M., Zellweger, C., Schwarzenbach, B., Bugmann, S., Buchmann, B., Ordóñez, C.,
1099 Prevot, A. S. H., and Hueglin, C.: Nitrogen oxide measurements at rural sites in Switzerland:
1100 Bias of conventional measurement techniques, *J. Geophys. Res.*, 112, 2006JD007971,
1101 <https://doi.org/10.1029/2006JD007971>, 2007.

1102 Suleiman, R.: TEMPO gridded NO₂ tropospheric and stratospheric columns V03
1103 (PROVISIONAL), https://doi.org/10.5067/IS-40E/TEMPO/NO2_L3.003, 2024.

1104 Thangavel, P., Park, D., and Lee, Y.-C.: Recent Insights into Particulate Matter (PM2.5)-
1105 Mediated Toxicity in Humans: An Overview, *IJERPH*, 19, 7511,
1106 <https://doi.org/10.3390/ijerph19127511>, 2022.

1107 Thiagarajan, P. and Ghosh, S.: Jensen–Shannon divergence based novel loss functions for
1108 Bayesian neural networks, *Neurocomputing*, 618, 129115,
1109 <https://doi.org/10.1016/j.neucom.2024.129115>, 2024.

1110 Toledo, A. S. O., Silini, R., Carpi, L. C., and Masoller, C.: Outlier mining in high-dimensional
1111 data using the Jensen–Shannon divergence and graph structure analysis, *J. Phys. Complex.*, 3,
1112 045011, <https://doi.org/10.1088/2632-072X/aca94a>, 2022.

1113 Tsigalou, C., Panopoulou, M., Papadopoulos, C., Karvelas, A., Tsairidis, D., and
1114 Anagnostopoulos, K.: Estimation of low-density lipoprotein cholesterol by machine learning
1115 methods, *Clinica Chimica Acta*, 517, 108–116, <https://doi.org/10.1016/j.cca.2021.02.020>, 2021.

1116 Urbanowicz, T., Skotak, K., Filipiak, K. J., Olasińska-Wiśniewska, A., Szczepański, K., Wyrwa,
1117 M., Sikora, J., Tykarski, A., and Jemielity, M.: Long-Term Exposure of Nitrogen Oxides Air
1118 Pollution (NO₂) Impact for Coronary Artery Lesion Progression—Pilot Study, *JPM*, 13, 1376,
1119 <https://doi.org/10.3390/jpm13091376>, 2023.

1120 2021 TIGER/Line® Shapefiles: [https://www.census.gov/cgi-
1121 bin/geo/shapefiles/index.php?year=2021&layergroup=Roads](https://www.census.gov/cgi-bin/geo/shapefiles/index.php?year=2021&layergroup=Roads), last access: 21 February 2025.

1122 U.S. 2020 Urban Areas Shapefile:
1123 https://www2.census.gov/geo/tiger/TIGER_RD18/LAYER/UAC20/, last access: 21 February
1124 2025.

1125 Van Der A, R. J., Eskes, H. J., Boersma, K. F., Van Noije, T. P. C., Van Roozendael, M., De
1126 Smedt, I., Peters, D. H. M. U., and Meijer, E. W.: Trends, seasonal variability and dominant NO_x
1127 source derived from a ten year record of NO₂ measured from space, *J. Geophys. Res.*, 113,
1128 2007JD009021, <https://doi.org/10.1029/2007JD009021>, 2008.

1129 Van Geffen, J., Boersma, K. F., Eskes, H., Sneep, M., Ter Linden, M., Zara, M., and Veefkind, J.
1130 P.: S5P TROPOMI NO₂ slant column retrieval: method, stability,
1131 uncertainties and comparisons with OMI, *Atmos. Meas. Tech.*, 13, 1315–1335,
1132 <https://doi.org/10.5194/amt-13-1315-2020>, 2020.

1133 Veefkind, J. P., Aben, I., McMullan, K., Förster, H., De Vries, J., Otter, G., Claas, J., Eskes, H. J.,
1134 De Haan, J. F., Kleipool, Q., Van Weele, M., Hasekamp, O., Hoogeveen, R., Landgraf, J., Snel,
1135 R., Tol, P., Ingmann, P., Voors, R., Kruizinga, B., Vink, R., Visser, H., and Levelt, P. F.:
1136 TROPOMI on the ESA Sentinel-5 Precursor: A GMES mission for global observations of the
1137 atmospheric composition for climate, air quality and ozone layer applications, *Remote Sensing*
1138 of Environment

1139 Venkatram, A.: Applications of Pollutant Frequency Distributions, *Journal of the Air Pollution
1140 Control Association*, 29, 251–253, <https://doi.org/10.1080/00022470.1979.10470788>, 1979.

1141 Virta, H., Ialongo, I., Szeląg, M., and Eskes, H.: Estimating surface-level nitrogen dioxide
1142 concentrations from Sentinel-5P/TROPOMI observations in Finland, *Atmospheric Environment*,
1143 312, 119989, <https://doi.org/10.1016/j.atmosenv.2023.119989>, 2023.

1144 Wang, F. and Zhang, Z.: Correlation Structure and Co-Movement of Hunan Province's Air
1145 Pollution: Evidence from the Multiscale Temporal Networks, *Atmosphere*, 14, 55,
1146 <https://doi.org/10.3390/atmos14010055>, 2022.

1147 Wang, Y., Bechle, M. J., Kim, S.-Y., Adams, P. J., Pandis, S. N., Pope, C. A., Robinson, A. L.,
1148 Sheppard, L., Szpiro, A. A., and Marshall, J. D.: Spatial decomposition analysis of NO₂ and

1149 PM2.5 air pollution in the United States, Atmospheric Environment, 241, 117470,
1150 <https://doi.org/10.1016/j.atmosenv.2020.117470>, 2020.

1151 Xia, X., Meng, X., Liu, C., Guo, Y., Li, X., Niu, Y., Lam, K. B. H., Wright, N., Kartsonaki, C.,
1152 Chen, Y., Yang, L., Du, H., Yu, C., Sun, D., Lv, J., Chen, J., Yang, X., Gao, R., Wu, S., Kan, H.,
1153 Chan, K. H., Li, L., Chen, Z., Chen, J., Chen, Z., Clarke, R., Collins, R., Li, L., Lv, J., Peto, R.,
1154 Walters, R., EdrisMohamed, A., Pozarickij, A., Iona, A., Wang, B., Clarke, C., Kartsonaki, C.,
1155 Schmidt, D., Avery, D., Bennett, D., Fry, H., Du, H., Lam, H., Turnbull, I., Millwood, I., Liu, J.,
1156 Clarke, J., Chan, K. H., Kolhe, K., Lin, K., Wang, L., Yang, L., Kakkoura, M., Rahmati, M.,
1157 Barnard, M., Mazidi, M., Wright, N., Yao, P., Ryder, P., Im, P. K., Harish, P., Nie, Q., Stevens, R.,
1158 Clarke, R., Walters, R., Boxall, R., Morris, S., Gilbert, S., Yang, X., Chen, Y., Chen, Z., Han, X.,
1159 Hou, C., Xia, Q., Liu, C., Lv, J., Pei, P., Sun, D., Yu, C., Pan, L., Pang, Z., Gao, R., Li, S., Duan,
1160 H., Wang, S., Liu, Y., Du, R., Zang, Y., Cheng, L., Tian, X., Zhang, H., Zhai, Y., Ning, F., Sun,
1161 X., Li, F., Lv, S., Wang, J., Hou, W., Sun, W., et al.: Associations of long-term nitrogen dioxide
1162 exposure with a wide spectrum of diseases: a prospective cohort study of 0·5 million Chinese
1163 adults, The Lancet Public Health, 9, e1047–e1058, [https://doi.org/10.1016/S2468-2667\(24\)00264-0](https://doi.org/10.1016/S2468-2667(24)00264-0), 2024.

1164

1165 Xu, A. and Xiang, C.: Assessment of the Emission Characteristics of Major States in the United
1166 States using Satellite Observations of CO₂, CO, and NO₂, Atmosphere, 15, 11,
1167 <https://doi.org/10.3390/atmos15010011>, 2023.

1168 Yan, J., Li, P., Gao, R., Li, Y., and Chen, L.: Identifying Critical States of Complex Diseases by
1169 Single-Sample Jensen-Shannon Divergence, Front. Oncol., 11, 684781,
1170 <https://doi.org/10.3389/fonc.2021.684781>, 2021.

1171 Yu, Z. and Li, X.: The Temporal–Spatial Characteristics of Column NO₂ Concentration and
1172 Influence Factors in Xinjiang of Northwestern Arid Region in China, Atmosphere, 13, 1533,
1173 <https://doi.org/10.3390/atmos13101533>, 2022.

1174 Zhang, R., Wang, Y., Smeltzer, C., Qu, H., Koshak, W., and Boersma, K. F.: Reconciling the
1175 differences between OMI-based and EPA AQS in situ NO₂ trends,
1176 <https://doi.org/10.5194/amt-2017-410>, 25 January 2018.

1177 Zhao, D., Yan, W., You, M., Zhang, J., Arun, P. V., Jiao, C., Wang, Q., and Zhou, H.:
1178 Hyperspectral Anomaly Detection Based on Empirical Mode Decomposition and Local
1179 Weighted Contrast, *IEEE Sensors J.*, 24, 33847–33861,
1180 <https://doi.org/10.1109/JSEN.2024.3455258>, 2024.

1181 Zoogman, P., Liu, X., Suleiman, R. M., Pennington, W. F., Flittner, D. E., Al-Saadi, J. A., Hilton,
1182 B. B., Nicks, D. K., Newchurch, M. J., Carr, J. L., Janz, S. J., Andraschko, M. R., Arola, A.,
1183 Baker, B. D., Canova, B. P., Chan Miller, C., Cohen, R. C., Davis, J. E., Dussault, M. E.,
1184 Edwards, D. P., Fishman, J., Ghulam, A., González Abad, G., Grutter, M., Herman, J. R., Houck,
1185 J., Jacob, D. J., Joiner, J., Kerridge, B. J., Kim, J., Krotkov, N. A., Lamsal, L., Li, C., Lindfors,
1186 A., Martin, R. V., McElroy, C. T., McLinden, C., Natraj, V., Neil, D. O., Nowlan, C. R.,
1187 O'Sullivan, E. J., Palmer, P. I., Pierce, R. B., Pippin, M. R., Saiz-Lopez, A., Spurr, R. J. D.,
1188 Szykman, J. J., Torres, O., Veefkind, J. P., Veihelmann, B., Wang, H., Wang, J., and Chance, K.:
1189 Tropospheric emissions: Monitoring of pollution (TEMPO), *Journal of Quantitative
1190 Spectroscopy and Radiative Transfer*, 186, 17–39, <https://doi.org/10.1016/j.jqsrt.2016.05.008>,
1191 2017.